NATIONAL AERONAUTICS AND SPACE ADMINISTRATION

APOLLO 7 MISSION REPORT

SUPPLEMENT 3

DRA

GUIDANCE, NAVIGATION, AND CONTROL
SYSTEM PERFORMANCE ANALYSIS

MANNED SPACECRAFT CENTER
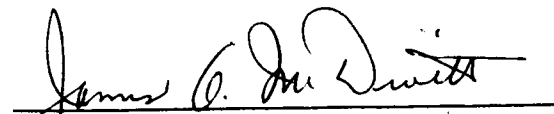## HOUSTON, TEXAS
NOVEMBER 1969

APOLLO 7 MISSION REPORT

SUPPLEMENT 3

GUIDANCE, NAVIGATION, AND CONTROL
SYSTEM PERFORMANCE ANALYSIS

PREPARED BY

TRW Systems Group

APPROVED BY

James A. McDivitt
Manager, Apollo Spacecraft Program

NATIONAL AERONAUTICS AND SPACE ADMINISTRATION

MANNED SPACECRAFT CENTER

HOUSTON, TEXAS

November 1969

PROJECT TECHNICAL REPORT

TASK E&D-38

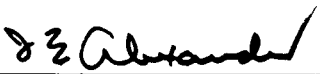**APOLLO VII GUIDANCE, NAVIGATION AND
CONTROL SYSTEM PERFORMANCE ANALYSIS - FINAL REPORT**

NAS 9-8166

20 DECEMBER 1968

Prepared for
NATIONAL AERONAUTICS AND SPACE ADMINISTRATION
MANNED SPACECRAFT CENTER
HOUSTON, TEXAS

Approved by _J ǯ Alexander_

J. E. Alexander, Manager
Guidance and Control
Systems Department

TRW
SYSTEMS GROUP

TABLE OF CONTENTS

LIST OF TABLES

LIST OF ILLUSTRATIONS

1. INTRODUCTION

1.1 GENERAL

This report contains the conclusion of the analyses of the inflight performance of the Guidance, Navigation and Control System of the AS-205/CSM-101/Apollo 7 spacecraft and is intended as a supplement to the MSC Mission Report for Apollo 7. Preparation and submittal of this report was accomplished under MSC/TRW Task E-38B, "Guidance and Control Test Analysis." Contributions to the analyses reported here-in were made under MSC/TRW Task E-72 and MSC/TRW Task A-50, "Trajectory Reconstruction." Specifically, Section 4 of this report, "Control System Evaluation," was prepared by the Task E-72 personnel. The inertial system evaluation and trajectory reconstruction tasks are highly interdependent, and Task A-50 personnel contributed significantly to Section 3.

The principal objective of the analysis depicted in Section 3 of this report was the determination of error sources present in the Apollo 7 Inertial Measurement Unit (IMU) during the flight. A description of the IMU error parameters considered appears in Table B-1. The parameters examined included platform misalignments, gyro and accelerometer errors, and accelerometer mounting errors. The errors were derived by comparison with the Best Estimate Trajectory (BET) during boost, orbital maneuvers and entry. The results of these analyses appear in Section 3.

Section 3 also contains a discussion of the results of a series of landmark tracking experiments performed during Apollo 7.

Section 4 presents discussions of several aspects of the control system performance that were imcomplete at the editorial deadline for the MSC Mission Report. The results are included here in the interest of completeness.

1.2 BACKGROUND

The Apollo 7 mission was the first manned flight of the Apollo series. The purpose of the flight was to demonstrate CSM operations and the capa-

bility of the spacecraft, crew and MSFN support facilities to conduct an earth orbital mission with the Apollo flight and ground hardware. The principal objectives of this mission having impact on the GN&C systems (in addition to fundamental spacecraft checkout and crew operations) was to perform transposition and simulated docking, and evaluate CSM active rendezvous activities. Overall spacecraft performance data and mission event times are presented in the MSC Mission Report for Apollo 7.

2. SUMMARY

The inertial subsystem performance parameters were determined by standard velocity comparison techniques using boost, orbital maneuver and entry data. A set of error terms was derived which provided a satisfactory fit to the observed performance of the subsystem. Although three of the derived error terms exceeded the one sigma tolerance established by system specifications, no adverse effect on mission performance was seen.

The control characteristics of the Block II spacecraft were successfully demonstrated. Automatic control of the spacecraft for attitude control, thrust vector control and entry stabilization were successfully accomplished. The flight data indicated that existing simulations of the entry control task in transsonic regions of flight are inadequate to accurately predict Reaction Control System (RCS) propellant consumption. Propellant margins were adequate for the flight in spite of the disparity between expected and actual flight performance.

3. ONBOARD NAVIGATION EVALUATION

Analysis of the Apollo 7 guidance and navigation system accuracy was based on satisfying several constraints simultaneously. These constraints were the velocity errors accrued during the boost to orbit phase, the measured biases for the accelerometers and gyros during flight, the entry altitude and descent rate conditions, and the calibration history of the inertial instruments during checkout at Kennedy Space Center prior to the launch. Using these constraints, a satisfactory set of error terms has been determined which made the G&N corrected trajectory fit the external measurements.

3.1 BOOST TRAJECTORY EVALUATION

The external reference used to generate the velocity comparisons used for these analyses was the Marshall Space Flight Center trajectory designated "Edited S-IVB IU-TM." This trajectory presents in the engineering judgement of TRW, the most realistic representation of the boost trajectory. The trajectory designated "Firal S-IVB Observed Mass Point Trajectory" normally the best estimate trajectory for the boost phase was considered, but rejected because of subtle differences in the trajectory characteristics near insertion, which required unmodelable G&N errors to fit satisfactorily.

The "Edited S-IVB IU-TM" is the MSFC estimate of the S-IVB guidance system indicated trajectory with telemetry dropouts corrected and known misalignments removed. As such, it may contain instrumental errors attributable to the S-IVB inertial guidance system. No allowance has been made for those errors: any that exist are included in the Apollo G&N errors. Comparison of the S-IVB insertions conditions with other trajectory sources indicate that these errors, if any, are small. For the purpose of this document, they are wrongfully attributed to the Apollo G&N system.

The analysis of the velocity differences was performed using the methodology outlined in Appendix B. The velocity differences before any compensation for errors appear in figures 3-1 through 3-3. The related position differences appear in figures 3-4 through 3-6. G&N error sources were selected to minimize these velocity differences.

Figure 3-1 Velocity Comparison
G&N Minus Edited SIVBIUTM X-Axis
3-2

Figure 3-2 Velocity Comparison
G&N Minus Edited SIVBIUTM Y-Axis
3-3
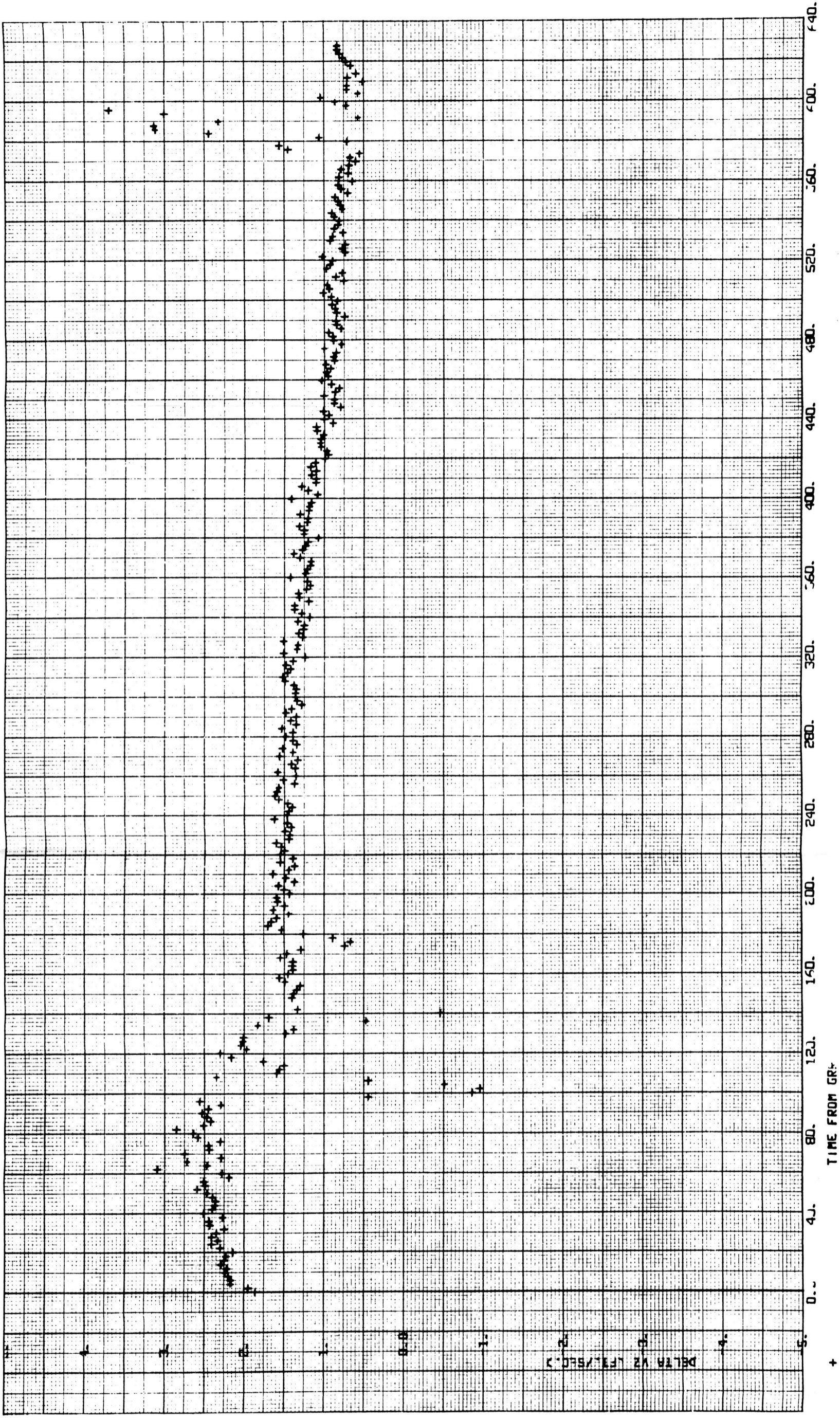
Figure 3-3 Velocity Comparison
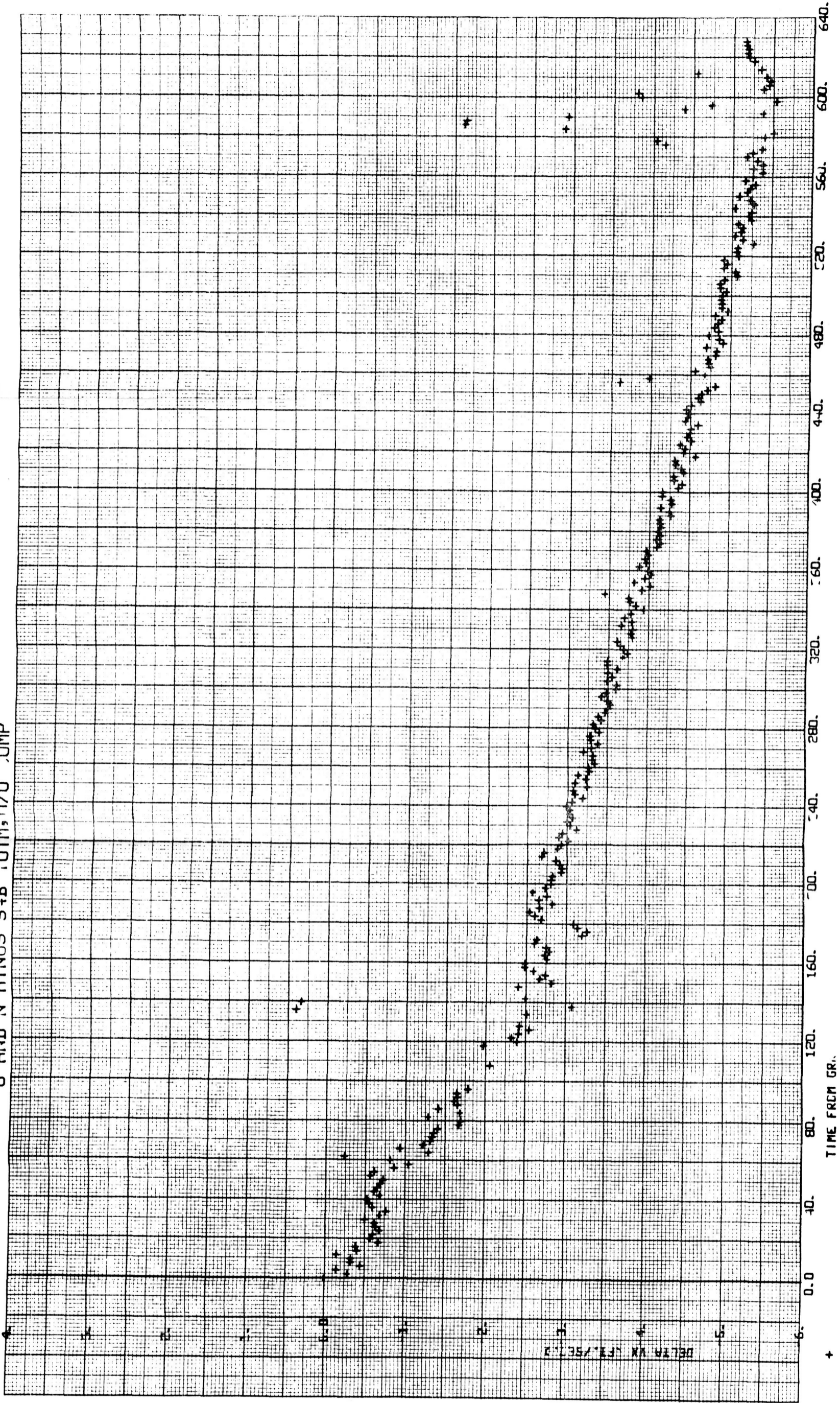G&N Minus Edited SIVBIUTM Z-Axis
3-4

Figure 3-4 Position Comparison
G&N Minus Edited SIVBIUTM X-Axis
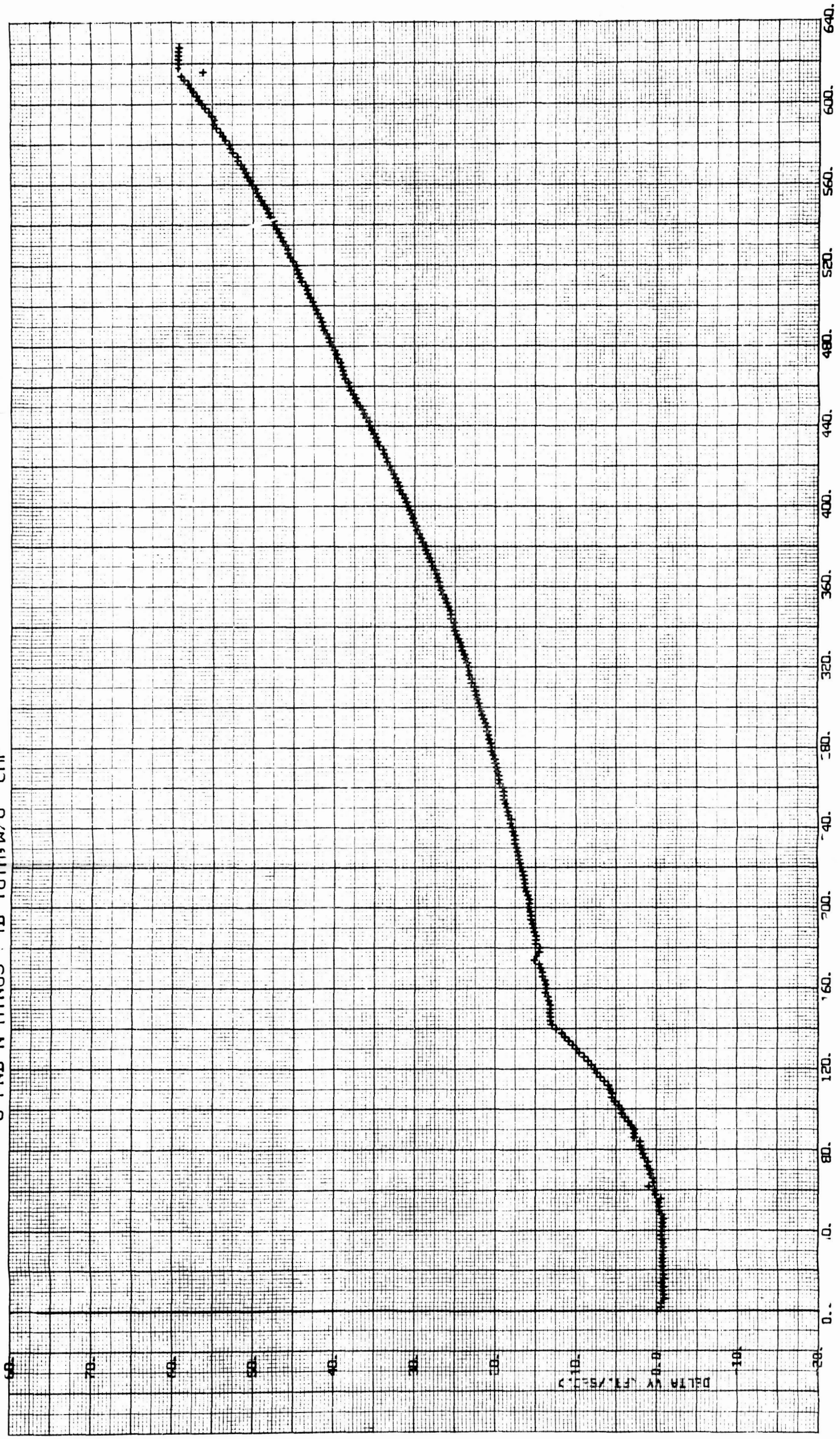3-5

G AND N MINUS S4B (UTM,W/O COMP
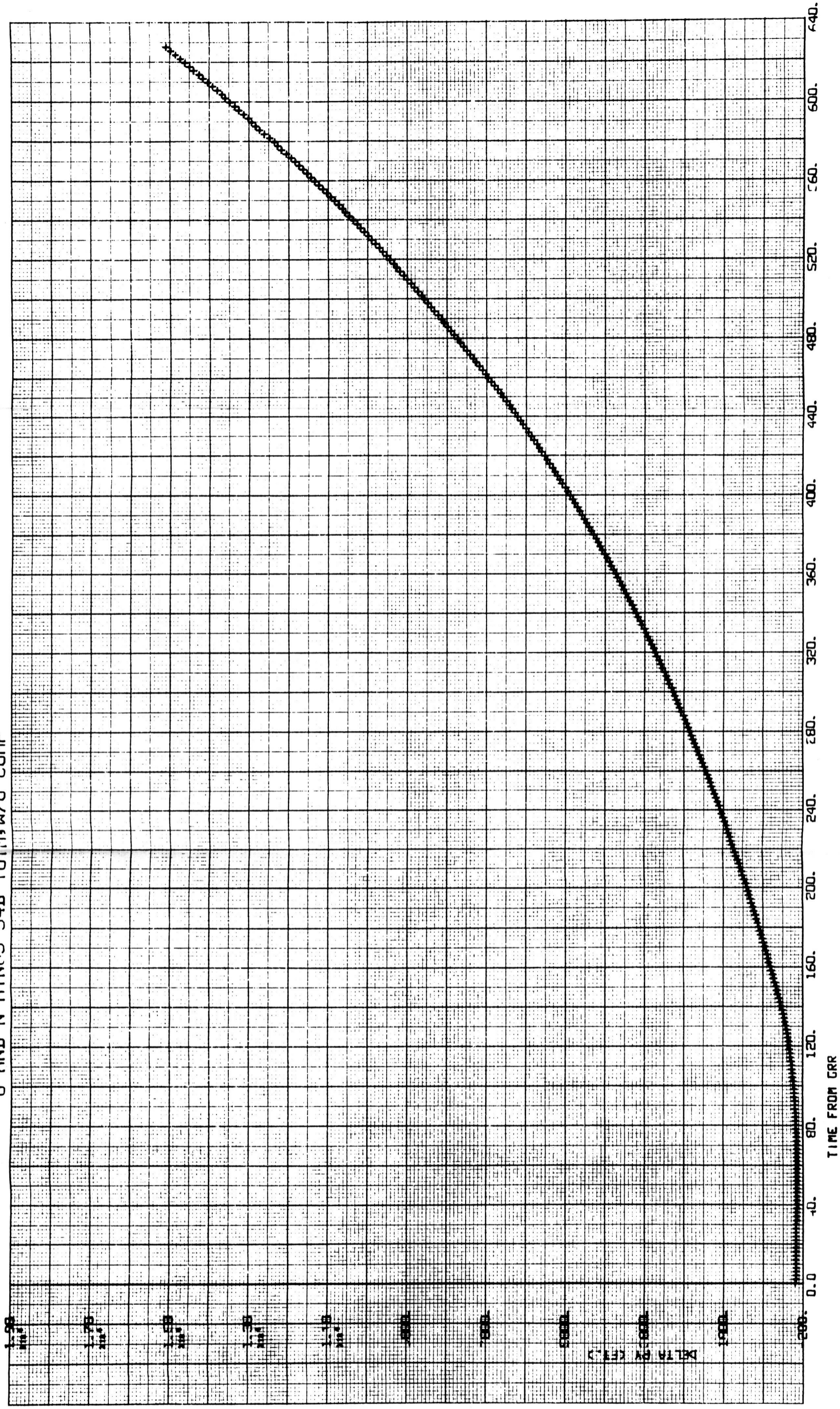
Figure 3-5 Position Comparison
G&N Minus Edited SIVBIUTM Y-Axis
3-6

G AND N MINUS S4B IUTM,W/O COMP
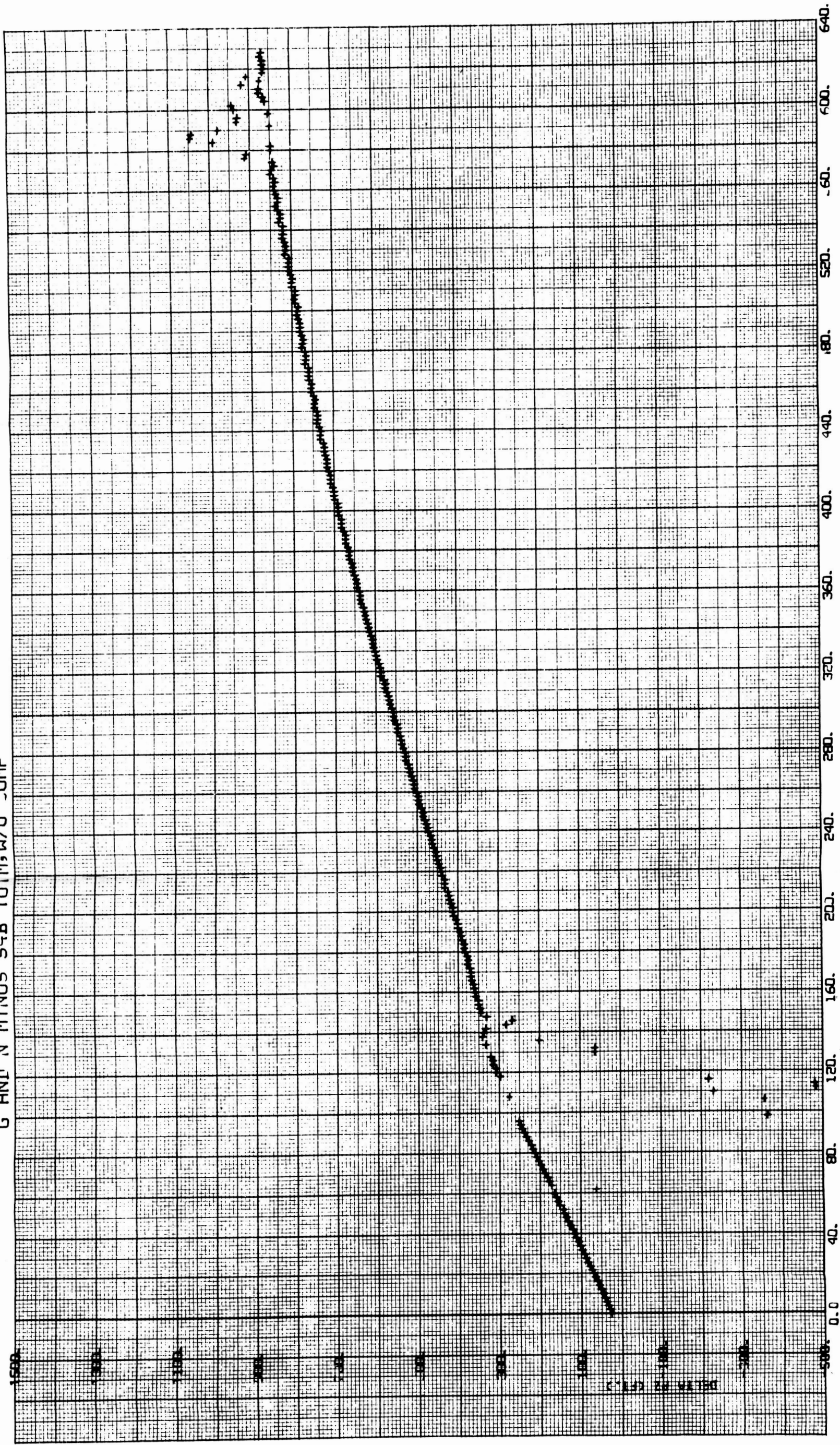
Figure 3-6 Position Comparison
G&N Minus Edited SIVBIUTM Z-Axis
3-7

The Z velocity offset resulted from the accumulated velocity of the spacecraft prior to computer recognition of lift-off (0.25 second after first motion). This delay accounts for the vertical velocity error.

The acceleration biases reflect the difference between the prelaunch estimate of bias, as loaded into the onboard computer for bias compensation, and those measured during flight. The Z-accelerometer scale factor error reflects the difference between the final calibrated value and the preflight load, adjusted to improve the fit to the flight data.

The gyro drift terms selected for the fit were chosen to satisfy three criteria. First, the Y-axis velocity error appears to be primarily influenced by the initial misalignment arising from X- and Y- gyro bias drift and by the Y- gyro acceleration sensitive drift due to acceleration along the spin reference axis. Next, the bias drift components were chosen to be consistent with the inflight measurements derived from successive (back-to-back) alignments. Finally, the dispersions of the parameters were constrained to be consistent with preflight calibration histories. The flight data only partially satisfied these constraints. The inflight bias drift measurements were plus 0.7, minus 1.8, and minus 0.2 meru for the X, Y, and Z gyros, respectively. These values compare favorably for the X- and Z- gyro fit parameters but differ significantly from the Y- gyro drift required to fit the velocity errors.

The acceleration sensitive drift terms (Table 3-I) indicates a significant deviation from the prelaunch calibrated values; the error terms were selected to optimize the fit to the velocity errors.

Early in the mission, observation of the Y-accelerometer register indicated that no accelerometer pulses were accumulating, although the preflight bias measurement showed 0.24 cm/sec^2. A small plus and minus Y-axis translation test verified that the accelerometer and associated electronics were functioning satisfactorily. Thus, it appeared the instrument bias had shifted from the preflight value to essentially zero. Subsequently, the onboard computer compensation for the bias term was updated to zero.

The most probable cause of the instrument bias shift is the null coincidence phemomenon. The accelerometer contains a pulse torquing loop designed to mode 3:3 at null. Some loops tend to change moding (dual

TABLE 3-1 IMU ERROR PARAMETERS, G&N MINUS EDITED S-IVB IU/TM

	Data Mean	Flight Load	Expected* Error	Standard Deviation (GSOP)	Expected 1σ Bounds		Derived Error Value
					Maximum	Minimum	
VOX (ft/sec)	N/A	N/A	N/A	N/A	N/A	N/A	.032
VOY (ft/sec)	N/A	N/A	N/A	N/A	N/A	N/A	.012
VOZ (ft/sec)	N/A	N/A	N/A	N/A	N/A	N/A	1.87
DT (sec)	0	0	N/A	N/A	N/A	N/A	- .0036
ACBX (cm/sec^2)	.20	.24	.04	.20	.24	- .158	.036
ACBY (cm/sec^2)	.25	.24	- .01	.20	.19	- .21	- .028
ACBZ (cm/sec^2)	.16	.17	.01	.20	.21	- .19	.01
SFEX (PPM)	-300	-306	6	116	122	-110	50
SFEZ (PPM)	-340	-408	- 68	116	48	-184	- 84
NBDX (MERU)	1.44	- .5	1.94	2	3.94	- .06	1.02
NBDY (MERU)	- .43	0	- .43	2	1.57	- 2.43	4.13
ADIAX (MERU/g)	10.4	8.2	2.2	8	10.2	- 6.8	- 12
ADIAY (MERU/g)	11.2	11.6	- .4	8	7.6	- 8.4	4.13
ADIAZ (MERU/g)	16.2	20.8	- 4.6	8	3.4	- 12.6	- 10.5
ADOAX (MERU/g)	N/A	N/A	N/A	2-5**	10	- 10	1.24
MLMX (arc-sec)	N/A	N/A	N/A	50	50	50	39
MLMY (arc-sec)	N/A	N/A	N/A	50	50	50	- 50
MLMZ (arc-sec)	N/A	N/A	N/A	500	500	-500	- 25

* Data mean minus flight load

** Recent unofficial MIT measurements

mode) near null, for example, from 3:3 to 2:2 (4:4). When this change
occurs, the bias for each mode is unique; this difference between the null
biases is called null coincidence and is manifested as an apparent instru-
ment dead zone that would mask a very small acceleration, either real
or bias. Preflight studies had determined that this dead zone might be
as much as 0.3 cm/sec^2 for some instruments; thus, the operational
instrument bias, determined preflight to be 0.24 cm/sec^2, would be lost
in the dead zone. This preflight bias is determined in a one-g field.
It is impractical in the system configuration to measure the zero-g null
bias; hence, the cumulative effects of environment and buildup of system
tolerances tended to degrade the null coincidence from the laboratory-
adjusted values determined for zero-g conditions.

During free-flight phases, the accelerometer bias can be determined
from the rate at which accelerometer pulses are accumulated in the accel-
erometer input registers. These results are contaminated by external
forces acting on the vehicle during flight, such as aerodynamic drag,
venting, and waste water dump, and by residual propulsive components from
attitude maneuvers with the center of mass displaced from the center of
rotation. The following table summarized the data from selected checks
of the inflight bias.

Time, hr:min		Bias, cm/sec^2		
From	To	X	Y	Z
4:39	4:52	0.275	0	0.215
142:55	144:20	0.318	0	0.209
144:20	145:05	0.294	0	0.208
142:55	145:05	0.309	0	0.208

The first check lasted for 13 minutes and was performed after spacecraft
separation from the S-IVB, but before any orbital maneuvers or system
shutdowns. The latter series of checks determined the biases for essen-
tially complete revolutions; using a complete revolution for bias deter-
mination would tend to remove the influence of aerodynamic drag but it
does increase the effects of other disturbing forces. The results of
these bias determinations are considered to be satisfactory. The inflight
bias determination made early in the flight was given maximum influence

in the launch velocity comparison analysis, since it would be least affected by subsequent shutdowns of the inertial system.

Successive (back-to-back) inertial system alignments determined the ability to measure zero-g bias drift. The inertial system was first aligned prior to the rendezvous maneuver. Several revolutions later, the gyro-torquing angles (the angles through which the stable member was moved to re-achieve the desired inertial attitude) were recorded. This test showed that the average stable member drift over that period was plus 0.7, minus 1.8, and minus 0.2 MERU, respectively, for the X, Y, and Z gyro axes. The results indicate that the inflight drift determination technique is satisfactory and that the stable member drift met mission requirements.

The error set derived to fit the boost errors, and constrained to satisfy the orbital maneuver evaluation and entry evaluation are shown in Table 3-I "Summary of System Errors." The velocity residuals resulting from a comparison of the Apollo G&N data, corrected for these errors, compared to the reference trajectory, "Edited S-IVB IU-TM," are shown in figures 3-7 through 3-9. The corrected position differences are shown in figures 3-10 through 3-12.

Table 3-I indicates statistical data from prelaunch calibrations of the Apollo IMU instruments. The time histories of the calibration data are shown in Appendix A "Preflight Calibration Histories." These data were extracted from TRW Project Technical Report 11176-H041-R0-00 "Apollo 7 GN&C Preflight Performance Summary," dated 20 September, 1968. They are included here as supplementary data. Also included in the calibration time histories are the prelaunch eraseable memory estimates of the error terms and the postflight evaluation solution.

3.2 ORBITAL MANEUVER RECONSTRUCTION

The SPS-5 burn (ΔV_S = 1695.45 ft/sec) was the only SPS firing large enough to afford a reasonable solution for platform misalignment angles from thrust velocity data. The IGS-ESPØD program was used to obtain the best-fit trajectory based on telemetered AGS PIPA data and MSFN tracking data before, during and after the burn. The solution indicated the following stable member misalignments:

3-11
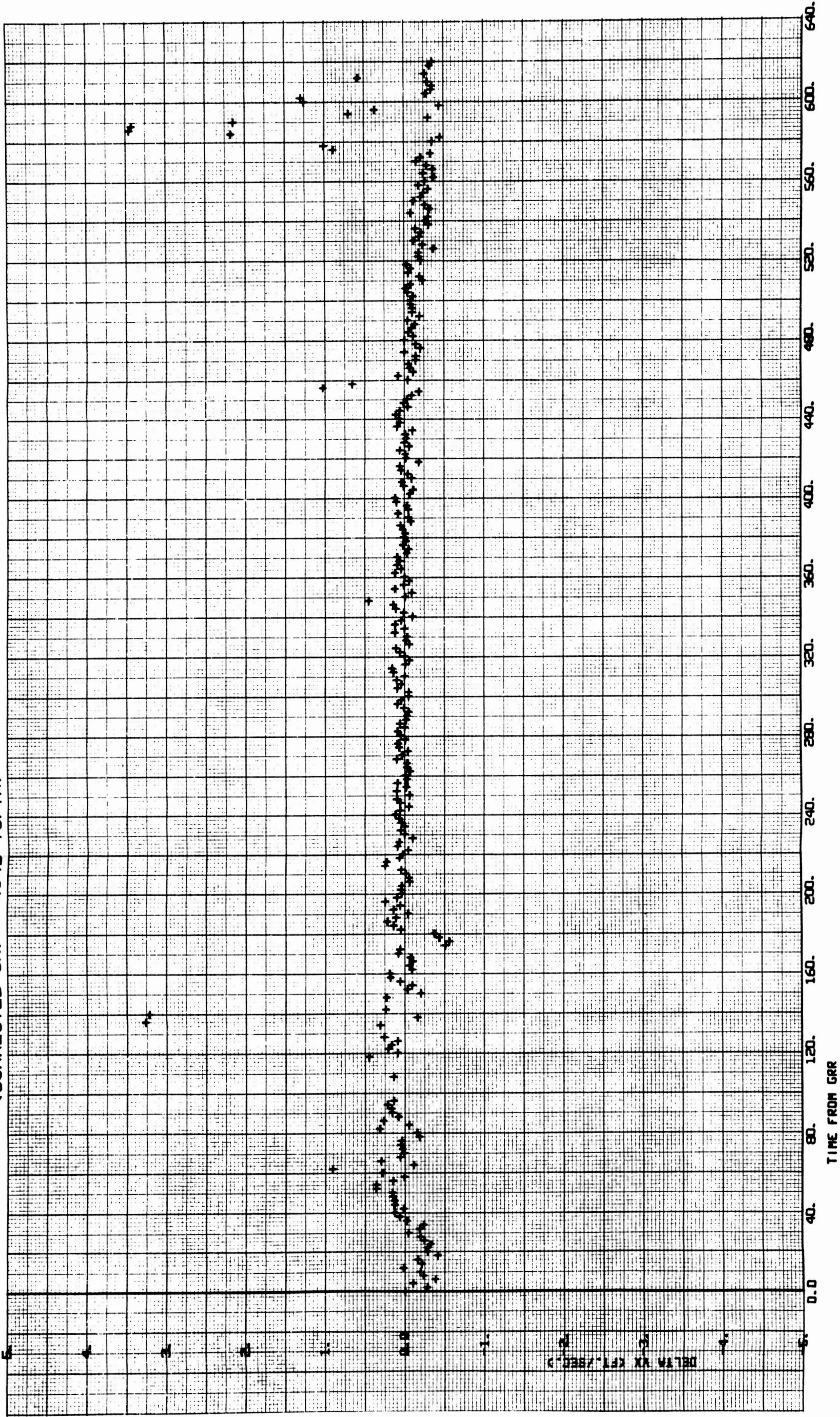
Figure 3-7 Velocity Residual Errors
Corrected G&N Minus Edited SIVBIUTM   X-Axis

3-12

<CORRECTED GN> - <S4B IU/TM>

DELTA VY (FT./SEC.)
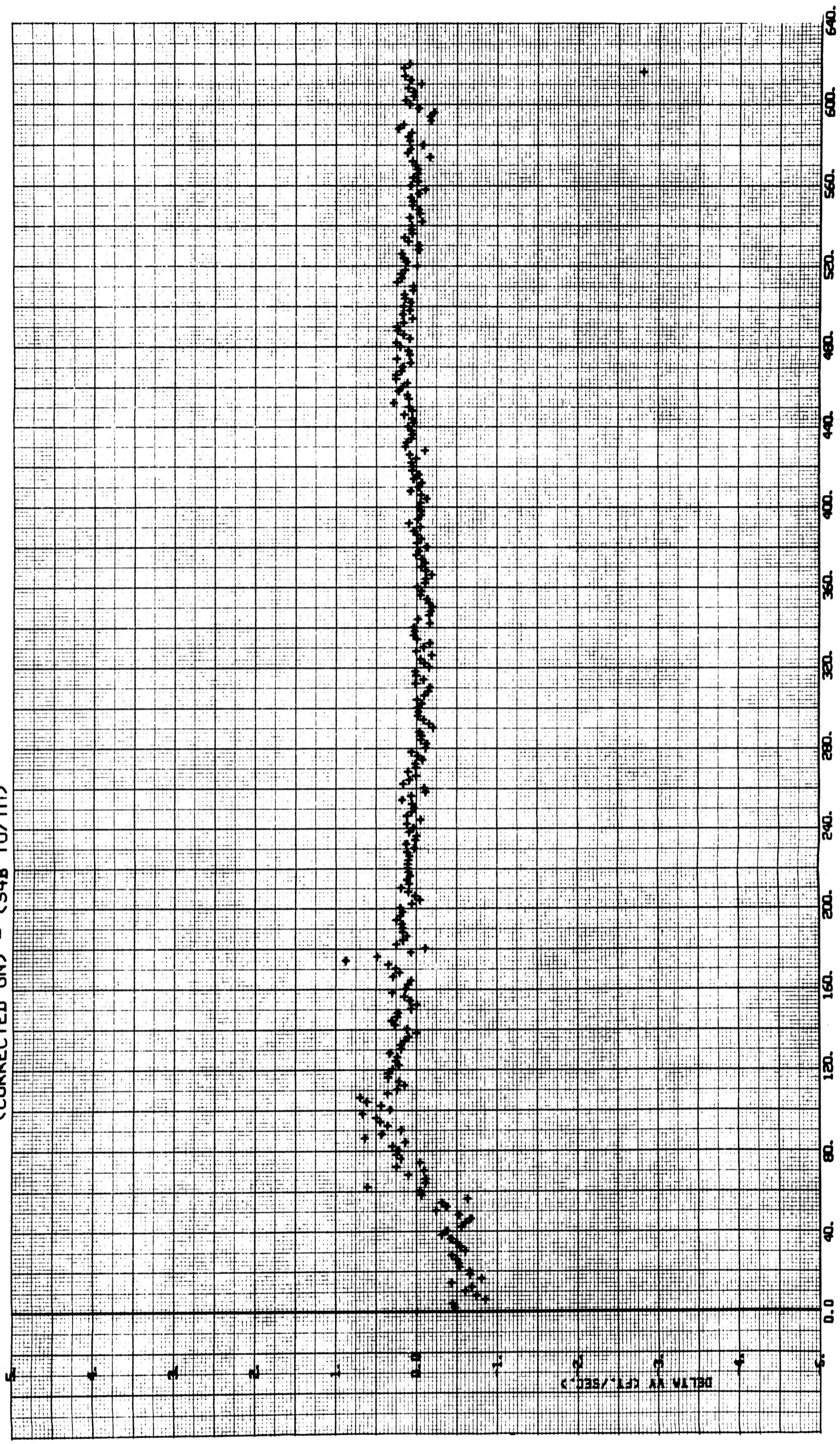
TIME FROM GRR

Figure 3-8 Velocity Residual Errors
Corrected G&N Minus Edited SIVBIUTM Y-Axis
3-13

Figure 3-9 Velocity Residual Errors
Corrected G&N minus Edited SIVBIUTM   Z-Axis

3-14
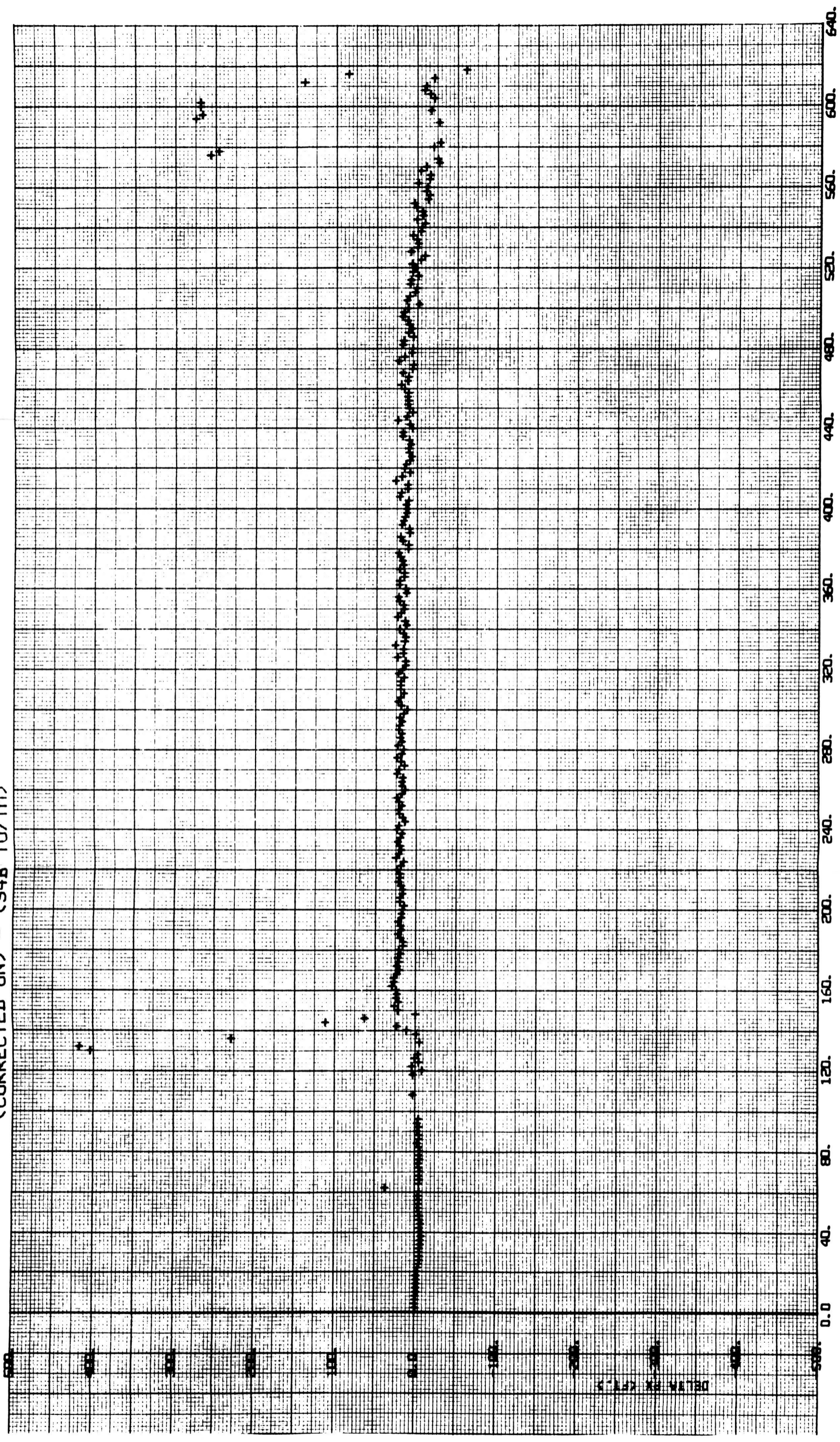
Figure 3-10 Position Residual Errors
Corrected G&N Minus Edited SIVBIUTM X-Axis
3-15
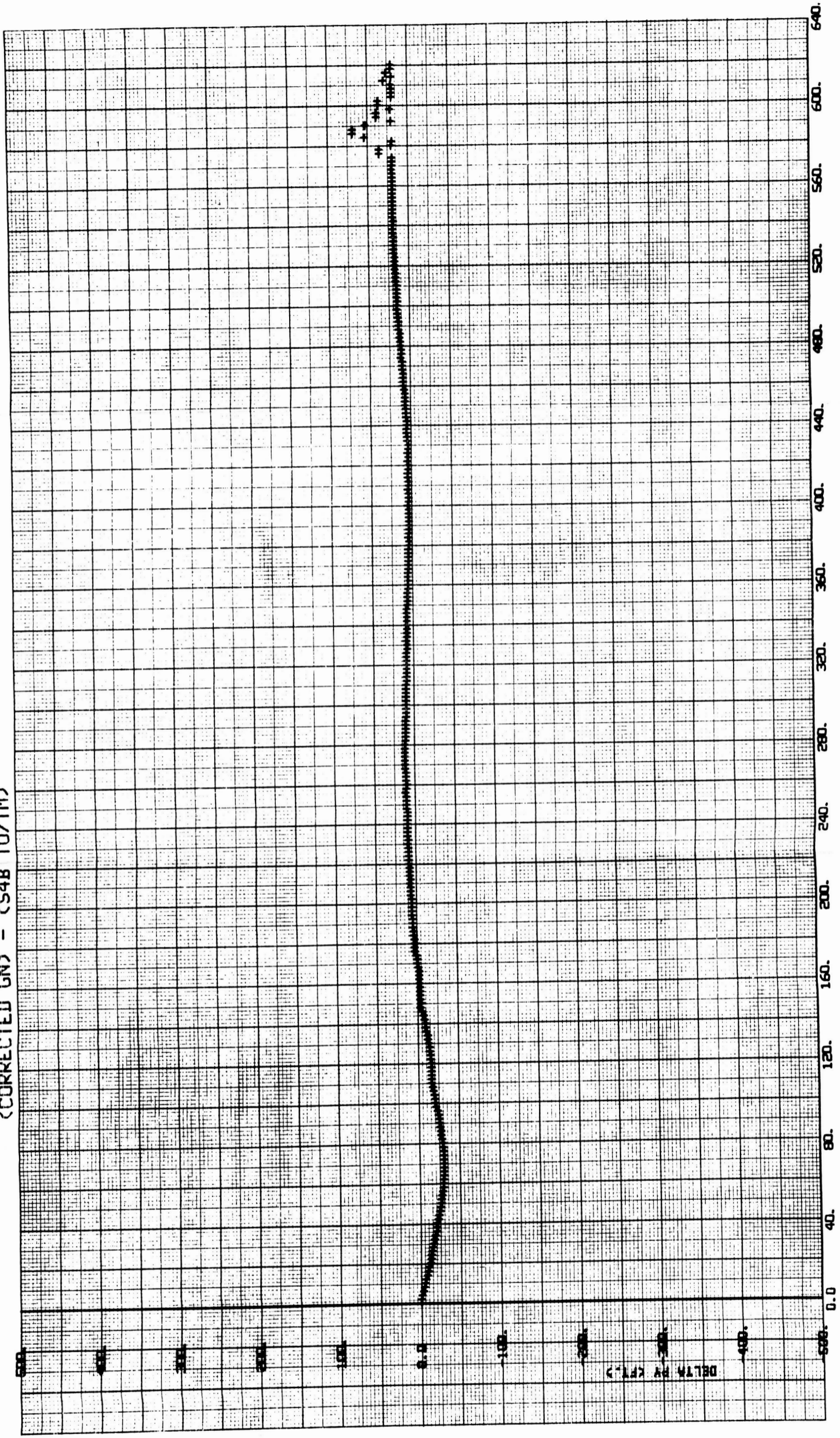
3-11 Position Residual Errors
Corrected G&N Minus Edited SIVBIUTM   Y-Axis
3-16
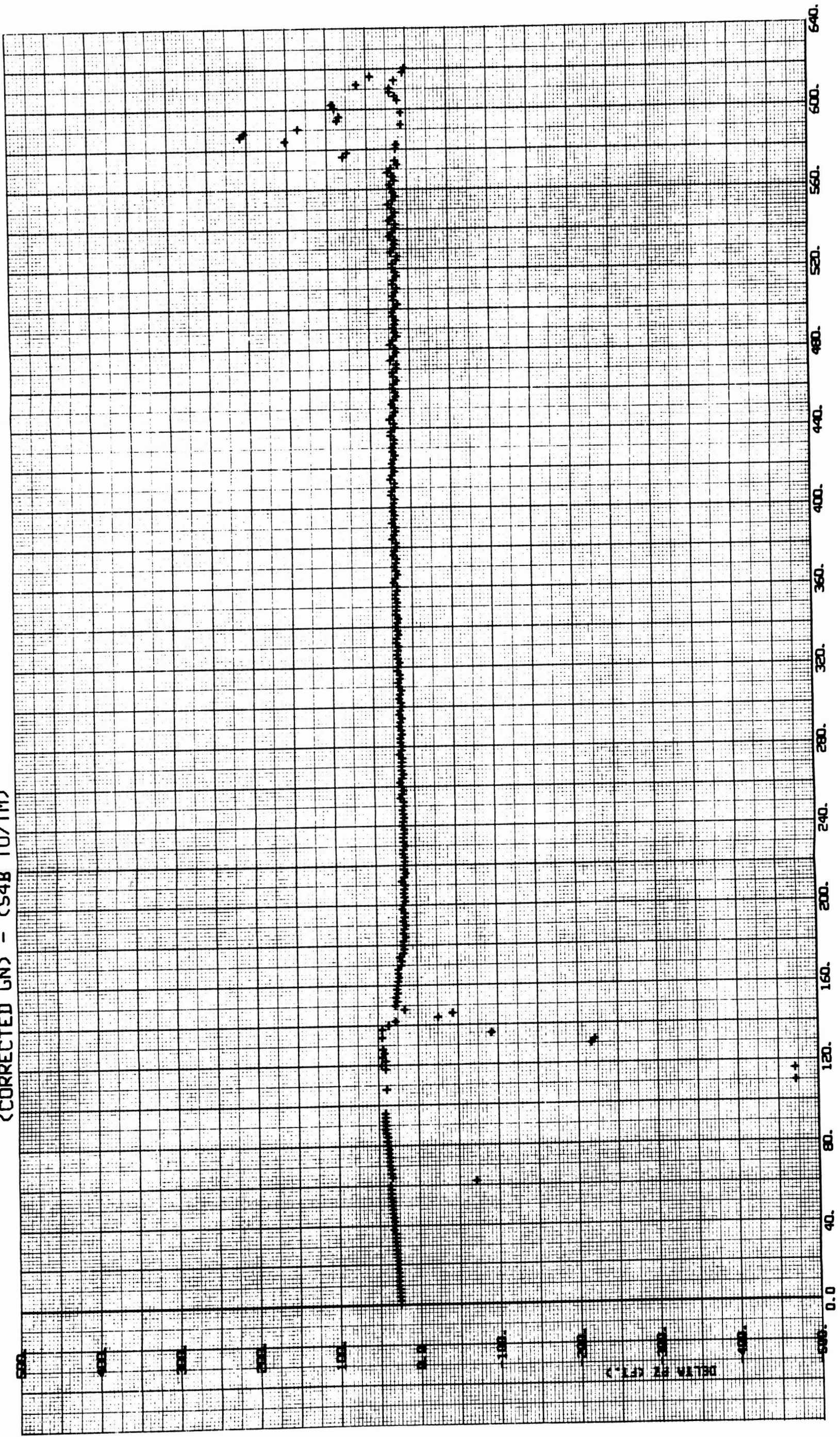
Figure 3-12 Position Residual Errors
Corrected G&N Minus Edited SIVBIUTM Z-Zxis

3-17

$$\emptyset_X = 0 \qquad \emptyset_Y = 73.6 \text{ sec.} \qquad \emptyset_Z = -51.9 \text{ sec}$$

These misalignments are compatible with the 1σ MEI Spec. for in-flight platform alignment errors (40 arc sec per axis).

The following table presents a comparison of the velocity increments in Apollo G&N platform coordinates actually applied, as measured by the ESPOD trajectory reconstruction, and the velocity increment as measured by the G&N System. These data indicate that the misalignments were inconsequential.

<div align="center">

VELOCITY COMPARISON

SPS-5 Burn
(ft/sec)

</div>

	V_{XS}	V_{YS}	V_{ZS}
Actual (ESPOD)	1693.41	14.01	81.24
Measured (G&N)	1693.41	14.44	81.84

3.3 ENTRY TRAJECTORY RECONSTRUCTION

The entry trajectory was initialized on the ESPOD BET state vector at t = 935600.77 sec GRR (approximately 6 sec before entry interface).

The 21-Day BET entry trajectory was corrected only for the Y-platform axis misalignment necessary to force the trajectory to fit the known altitude constraints. The required misalignment was $\emptyset_Y =$ 135.5 sec.

Another fit was obtained using the ascent errors (Table 3-I) plus a Y-axis platform misalignment of $\emptyset_Y = 90.0$ sec.

The results of these reconstructions are summarized in Table 3-II

The corrected entry trajectory shows acceptable comparison considering that it is the result of an open loop propagation of guidance data for over fifteen minutes. The differences are attributable in part to uncertainty in the initial conditions. Errors in the initial position propagate into relatively large errors in position and velocity at impact.

Table 3-II   COMPARISON OF ENTRY PARAMETERS

EVENT	TIME Sec GRR	KNOWN CONSTRAINT	21-DAY BET	ASCENT ERRORS
Drogue Chute Deployment	936201.6	Altitude* $H = 24000$ ft $\pm$ 5%	25200 ft	25790 ft
Main Chute Deployment	936252.6	Altitude* $H = 10500$ ft $\pm$ 5%	12300 ft	12490 ft
Splashdown	936526.77**	Altitude** $H = 600$ ft	612 ft	677 ft
		Descent Rate (Nom.) $V_H = 28$ ft/sec	35 ft/sec	35 ft/sec

* Pilots Altimeter

** Time at which DSE tape ran out. Altitude estimate is based on nominal descent rate and actual splash-time of 936547.6 sec.

3-19

The various estimates of the coordinates of the splashdown point are shown in the table below. These results are also plotted in Figure 3-13.

SPLASHDOWN COORDINATES

	Planned	Recovery Ship Est.	BET
Latitude	27.6333 deg	27.541 deg	27.6093 deg
Longitude	-64.1667 deg	-64.007 deg	-64.1318 deg

3.4 ESPOD

The principal source of trajectory information after CSM/Booster separation is the ESPOD trajectory reconstruction program. This program is a comprehensive model of the principal and disturbing accelerations which act on the spacecraft during free fall (non-thrusting, exoatmospheric flight). As such, it is used to generate a continuous estimate of the free fall trajectory of an orbiting spacecraft based on radar data and models of the earth potential field, aerodynamic drag, solar, lunar and planetary perturbations, and radiation pressure.

3.5 TIMING

The time base used in the velocity comparisons and guidance trajectory analyses in this report is CMC time, which is referred to Apollo G&N guidance reference release. This time base is used exclusively in the guidance analysis and velocity comparison computer programs.

In order to convert the time base used in this report to Range Time or Ground Elapsed Time (GET) a constant bias of 0.42 seconds should be added to the times in this section.

3.6 INERTIAL SUBSYSTEM ERROR ANALYSIS

Of the forty error terms modeled for the Apollo Inertial Subsystem analysis (see Table B-1 for a complete listing of errors) only three exceeded the one sigma tolerance established by the system specification. None of these errors nor any of the others that fell within system tolerances had a deleterious effect on the performance of the inertial subsystem throughout the flight of APOLLO VII. Although several power-down-

Figure 3-13 SPLASHDOWN POINT ESTIMATES

LATITUDE DEGREES NORTH

27.64
27.62
27.60
27.58
27.56
27.54
27.52

-64.00
-64.02
-64.04
-64.04
-64.06
-64.10
-64.12
-64.14
-64.16
-64.18

LONGITUDE DEGREES EAST

A

E

D

C-Sonant
D-RCS
A-Recovery Ship
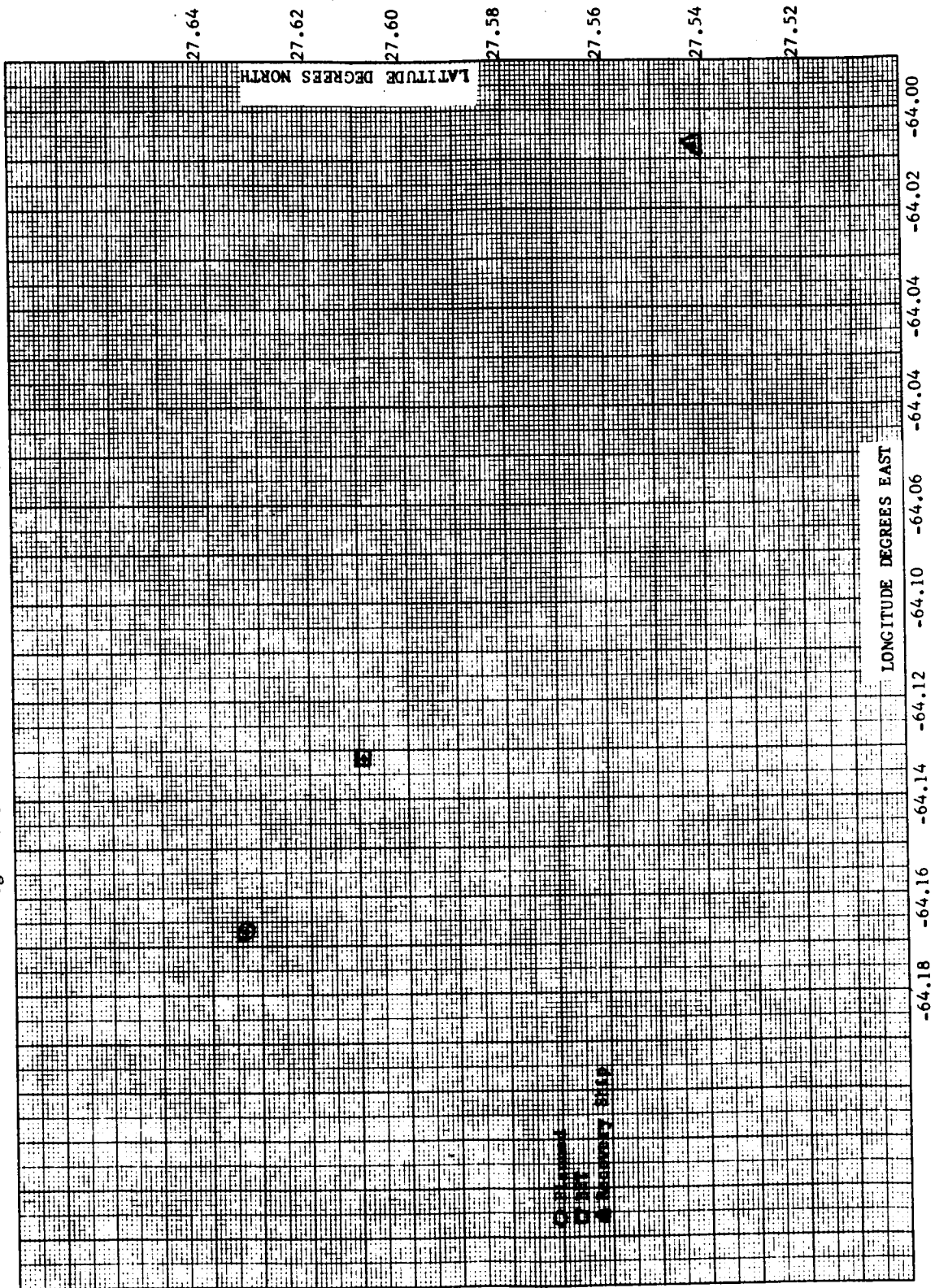
power-up sequences were performed during the Apollo 7 Mission, no shifts
in inertial instrument performance parameters were noted.

The following sections discuss the error terms which exceeded the
system performance specification.

3.6.1 Acceleration Sensitive Drift of the Z-Axis Gyro Due to Acceleration Along the Input Axis (ADIAZ)

The results of the analysis shown in this report indicated that ADIAZ
differed from the prelaunch estimated value (prelaunch load) by minus 10.5
meru/g compared to the specification values of $\pm$ 8 meru/g. This variation
can be explained in part by an apparent erroneous estimation of the term
preflight. The preflight mean value for this term was 16.2 meru/g con-
trasted with the preflight load of 20.8 meru/g. If this 4.6 meru bias is
considered, the inflight measured value falls within expected tolerance.

3.6.2 Acceleration Sensitive Drift of the X-Axis Gyro Due to Acceleration Along the Input Axis (ADIAX)

Nothing in the preflight test history of ADIAX satisfactorily ex-
plains the large deviation noted in ADIAX in the flight data. This term
is rather insensitive in the derivation of the inertial system errors.
Although this drift term is exercised quite heavily by the thrust during
boost, the velocity accrued late in the ascent profile in the Y and Z axes
is small, making the exact drift difficult to define. While the error
term shown is larger than the one sigma specification, it carries a
relatively large uncertainty. The -12 meru/g value was selected because
it optimized the fit to the velocity residuals.

3.6.3 Non-Compensated Bias Drift of the Y-Gyro (NBDY)

The Y-gyro bias drift presents another paradox. The preflight cali-
brations of this term were very well-behaved. The preflight estimate used
in the prelaunch load approximated very closely the mean of the prelaunch
calibrations. The measurement of platform drift during the flight
indicated a minus 1.8 meru drift. Each of the velocity comparisons
attempted yielded a positive value of this drift term. Both SPS burn 5
and entry trajectory reconstruction required a positive Y-axis misalign-
ment to fit the external reference data. These data, as well as the fit
to the boost trajectory, dictated the selection of 4.13 meru as the error
in NBDY.

3.7 OPTICAL SUBSYSTEM EVALUATION

3.7.1 Landmark Tracking

Landmark tracking data were processed in the following manner.

Mark data were collected from the downlinked computer words tab listings. Computer values used were mark time, shaft and trunnion angles at mark time, X, Y, Z CDU's at mark time and REFSMMAT. These values were used to compute a unit vector in the landmark to CSM direction and transform the vector to an earth centered reference coordinate system. A weighted least squares procedure was used to arrive at a best estimate for this pointing vector from all the mark data taken on a given landmark. Ephemeris data was taken from the TRW NAT BET. Six points, at 30 second intervals which spanned the mark time interval for a given landmark were used to interpolate for CSM state vectors at the specific mark times. An iterative process was used to adjust latitude and longitude until the computed adjustment was below some predetermined epsilon. Changes in latitude and longitude, from input values to computed values are shown in Tables 3-III and 3-IV.

The first five entries in Table 3-III were tracked during Revs. 90 through 92. Five marks were taken on each landmark with the exception of the unknown landmark in which case there were only three marks available. Data for the time interval immediately preceding the first available mark were missing consequently it is unknown whether more marks were taken or not on the unknown point.

The last three entries in Table 3-III were tracked during Revs. 135/136. Landmark 225 was tracked in both sets of data and is differentiated in the second set by 225*. The increase in delta latitude and longitude during the second period of tracking is unexplained. Perhaps lighting or a change in personnel caused a different point to be tracked. Note in Table 3-VI that the RMS residuals are much larger for LMK 225*. Also, only four marks were available for LMK 225* while five marks were available for the rest of the targets in the second set.

It should be noted that the residuals shown in Table 3-VI indicate angular deviations of the pointing vectors and should not be compared to changes in latitude and longitude.

3-23

The sensitivities indicate that a change in CSM position in cross range or downrange translates to an equal change in landmark location. A change in altitude has very little effect on the landmark location.

A guesstimate of the change in latitude and longitude, that would result from an error in the pointing vector direction of a magnitude equal to the RMS residuals from Table 3-VI, indicates that the change is roughly of the same order of magnitude as the deltas from 3-III. (Assuming a students T distribution and five data points the true value lies within one sigma of the mean with 90% confidence.)

The following is a description of the data contained in Table 3-III through 3-VI.

Table 3-III

    Col. 1. Landmark identification number

    Col. 2. Estimated error of surveyed location of the landmark taken from survey data sheets, units-feet.

    Col. 3. Input latitude obtained from downlinked DSKY display and converted from geodetic to geocentric to use in the computer program units-degrees.

    Col. 4. Horizontal displacement estimate caused by adjusting the latitude of the landmark (Δ Lat x 60 x 6000) units-feet.

    Col. 5. Delta latitude (adjusted - input) units-degrees.

    Col. 6. Input longitude obtained from downlinked DSKY display. Units-degrees.

    Col. 7. Horizontal displacement estimate caused by adjusting the longitude of the landmark (Δ Long x 60 x 6000 x Cos(Lat) units-feet

    Col. 8. Delta longitude (adjusted-input) units-degrees.

Table 3-IV contains the delta latitude and delta longitude resulting from perturbations in the BET state vectors representing 500 ft. changes in downrange, crossrange and altitude. Plus a timing change of 0.05 seconds in mark time. Delta's are computed Best Estimate-Input.

Col. 1   Landmark identification number.

Col. 2   Delta latitude and delta longitude with + 500 ft.
and 3   in the down range direction.

Col. 4   Delta latitude and delta longitude with 500 ft.
and 5   in the cross range direction.

Col. 6   Delta latitude and delta longitude with 500 ft.
and 7   in altitude.

Col. 8   Delta latitude and delta longitude with + 0.05
and 9   seconds in mark time.

Col. 10   Delta latitude and delta longitude with large (10,000
and 11   ft.) error in down range directions (LMK No. 11 has
           10,000 ft error in altitude).

Comparison of the deltas from Table 3-III to the deltas from Table 3-IV gives an estimate of the sensitivity of landmark location to errors in ephemeris data.

Table 3-V

Col. 1   Landmark identification number

Col. 2   Delta latitude with .4 milliradian error in
          shaft angle.

Col. 3   Delta longitude with .4 milliradian error in
          shaft angle.

Col. 4   Same as Col.'s 2 and 3 except with a .5 milliradian
and 5   trunnion angle error and no shaft angle error.

Comparison of the deltas from Table 3-V to the deltas from Table 3-III gives a estimate of the sensitivity of landmark location to errors in shaft and trunnion angles.

Table 3-VI

Col. 1   Landmark identification number.

Col. 2   RMS residuals in terms of hour angle and declination
and 3   for the unit vectors described above. (Since the unit
          vectors are in the opposite direction to the pointing
          vector, this is a measure of the accuracy with which
          the pointing direction can be determined.)
          Units-radians.

Col. 4   Same as Col. 2 and 3 except units are degrees.
and 5

TABLE 3-III

LMK Number	Horizontal Error	Latitude (Input) (Geocentric)	Horizontal Displacement ΔLat x 60 n.m x 6000 ft/n.m.	Δ Latitude Best Estimate Input	Longitude Inputs	Horizontal Displacement ΔLat x 60 n.m. x 6000 ft/n.m.	Δ Longitude Best Estimate Input
10	653 ft.	28.714	2340	- .0065	- 112.585	1140	.00356
8	2713 ft	27.693	2700	- .0075	- 115.081	1260	.0008
Unknown		30.500	500	.0014	- 100.988	4060	- .0131
225	948 ft	-22.744	610	.0017	14.444	930	- .0028
48	98 ft	25.516	290	- .0008	- 80.158	880	- .0027
225*	948 ft	- 22.744	5180	.0144	14.444	13,340	- .0402
11	653 ft.	27.680	1800	.0050	- 110.884	260	.0008

Table 3-III Landmark Location

TABLE 3-IV

	500 FT. DOWN RANGE		500 FT. CROSS RANGE		500 FT. ALTITUDE		-.05 SEC. EPHEMERIS	
	Δ Latitude	Δ Longitude	Δ Latitude	Δ Longitude	Δ Latitude	Δ Longitude	Δ Latitude	Δ Longitude
10	-.0067	.0051	-.0052	-.0038	.0065	-.0035	-.0071	.0076
8	-.0071	.0023	-.0061	-.0004	-.0075	.0008	-.0065	.0045
209	.0006	.0115	.0024	.0110	.0012	.0103	-.0005	.0133
Unknown	.0013	-.0115	.0027	-.0130	.0014	-.0131	.0011	-.0092
225	.0011	-.0014	.0029	-.0022	.0017	-.0028	.0003	.0005
48	-.0012	-.0013	.0005	-.0023	-.0008	-.0027	-.0020	-.0011
225*	.0139	-.0388	.0157	-.0397	.0144	-.0402	.0131	-.0366
11	.0046	.0023	.0063	.0012	.0050	.0008	.0040	.0048

Table 3-IV Landmark Location Changes Due to Ephemeris Changes

TABLE 3-V

LANDMARK	SHAFT ANGLE ERROR OF .4 M.R.		TRUNNION ANGLE ERROR OF .5 M. R.	
	Δ Latitude	Δ Longitude	Δ Latitude	Δ Longitude
10	- .0068	.0030	- .0060	.0027
8	- .0073	.0010	- .0074	.0004
209	.0011	.0103	.0016	.0098
Unknown	.0015	- .0133	.0012	- .0137
225	.0017	- .0030	.0025	- .0030
48	- .0010	- .0024	- .0006	- .0033
225*	.0139	- .0400	.0148	- .0405
11	.0049	.0012	.0050	.0005

Table 3-V Landmark Location Changes Due to Shaft and Trunnion Errors

TABLE 3-VI

RMS Residuals for each landmark.

LMK	Hour Angle (Radians)	Declination (Radians)	Hour Angle (Degrees)	Declination (Degrees)
10	.0009	.0017	.0512	.0974
8	.0007	.0020	.0401	.0013
209	.0011	.0013	.0630	.0745
Unknown	.0009	.0014	.0512	.0802
225	.0018	.0009	.1031	.0512
48	.0006	.0007	.0343	.0401
225*	.0037	.0039	.2120	.2235
11	.0023	.0013	.1318	.0745

Table 3-VI Pointing Direction Residuals

3-29

3.7.2 IMU Alignment

Analysis of alignment errors was not attempted for the following reasons.

Check sightings were not made after an alignment and mark data were not downlinked during the coast and align phases. Computed star vectors were available but mark times, shaft, trunnion and CDU angles at mark times were not. The net result was to preclude any statistical analysis of shaft, trunnion and CDU angles or astronaut errors except by inference from the results of burns with the platform aligned by star sightings. These results are covered elsewhere and are not included here.

4. CONTROL SYSTEM EVALUATION

This section of the report presents the evaluation of the Digital Autopilot of GN&C System. Subsections present in detail the evaluation of the attitude control function, the thrust vector control function and the stabilization of the command module during entry. In addition, the attitude control function of the Stabilization and Control System is discussed.

4.1 RCS DAP ATTITUDE CONTROL

Several -X and +Z translation maneuvers were executed during CSM-S-IVB rendezvous with the RCS DAP configured for narrow deadband attitude hold. DAP performance was satisfactory throughout the sequence of maneuvers. At GET 1:05:31:05.25, CSM RCS jets 3, 4, 7 and 8 fired initiating a four jet -X translation. X axis velocity to be gained at initiation of the maneuver was -4.5 ft/sec. A disturbance acceleration of 0.5 deg/sec^2 was observed in the pitch axis while the -X translation was in progress. CSM RCS jet number three was correctly turned off by the DAP 1.3 seconds after initiation because the pitch attitude error reached the 0.5 degree deadband. Pitch axis angular acceleration with jet three turned off was -.43 deg/sec^2. This value of acceleration indicates that jet 4 of the CSM RCS was achieving approximately 50% of nominal torque. The reduction in effective torque resulted from jet impingement on the CM/SM umbilical cover. The ullage ended 2.4 seconds after initiation.

Three additional four jet, -X translation maneuvers were performed at GET 1:05:31:08.6, 10.3 and 12.4 with durations of 0.9, 1.0 and 0.5 seconds respectively. All three maneuvers required RCS jet number three to be turned off periodically to counteract the pitch axis disturbance torque. The X axis velocity to be gained at the end of this sequence of maneuvers was -2.4 ft/sec.

At GET 1:05:31:18.9 a plus Z translation maneuver was initiated by the firing of RCS jets 9 and 10. Z axis velocity to be gained at ullage initiation was 0.7 ft/sec. RCS jet number 10, (minus roll, plus Z) was turned off for minimum impulse duration five times during the maneuver as the roll attitude error approached the five degree deadband. A pitch axis angular acceleration of .27 deg/sec^2 required the firing of minus pitch jets during the maneuver. This acceleration is attributed

to the center of mass being offset from the plane of action of the RCS
jets. The Z axis translation ended 3.4 seconds after initiation. Z
axis velocity to be gained at the end of the ullage was +0.1 ft/sec.

In summary, the RCS DAP successfully performed the attitude hold
mode function according to phase plane design during ullages in two
axes. Testing was quite brief as DAP attitude hold was performed less
than 30 seconds. DAP response to THC command inputs and jet selection
including rotational over translational priority was verified to a
limited extent as described above.

4.2 SCS ATTITUDE HOLD TEST

During SPS cold soak, the SCS was tested in minimum deadband, high
rate attitude hold. Figures 4-1, 4-2 and 4-3 present phase plane plots
of approximately five minutes of the test. The plots were constructed
from oscillograph data. The switching line for the minimum deadband,
high rate configuration intercepts 4.0 degrees attitude error for
zero rate and 2 deg/sec rate for 0.0 degrees attitude error.

Allowing for errors in recording and measuring oscillograph data,
all RCS jet firings were in accordance with the SCS phase plane design
in the minimum deadband, high rate configuration, indicating nominal
performance of the SCS Attitude Hold function.

4.3 TVC DAP PERFORMANCE

Eight Service Propulsion System maneuvers were executed during the
Apollo 7 mission. Of these, six were controlled by the G&N System, in-
cluding two minimum impulse (half-second) burns, and the manual takeover,
and two were controlled by the Stabilization and Control System.

These eight SPS burns are identified by downlink data source, time
of ignition and burn duration. A fairly detailed description of engine
angles and computer trim estimates is presented along with an extensive
table of trim activity. Attitude errors resulting from the mistrims
and other distrubances are discussed in the first section on autopilot
performance.

4.3.1 Autopilot Performance During SPS Burns

Autopilot performance was excellent for all SPS burns during Mission
C. Peak attitude errors during SCS controlled burns were about one degree
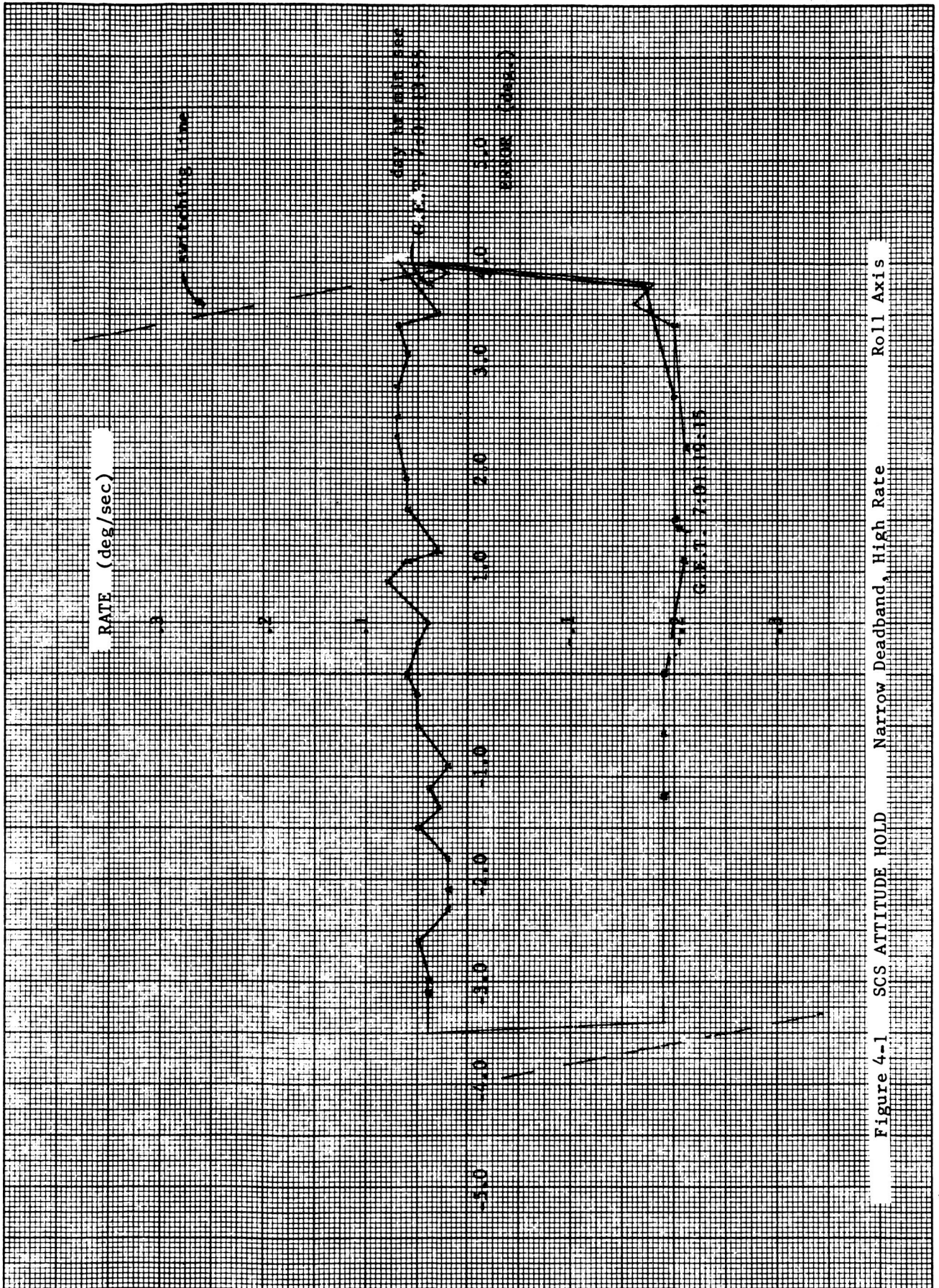
Figure 4-1   SCS ATTITUDE HOLD   Narrow Deadband, High Rate   Roll Axis
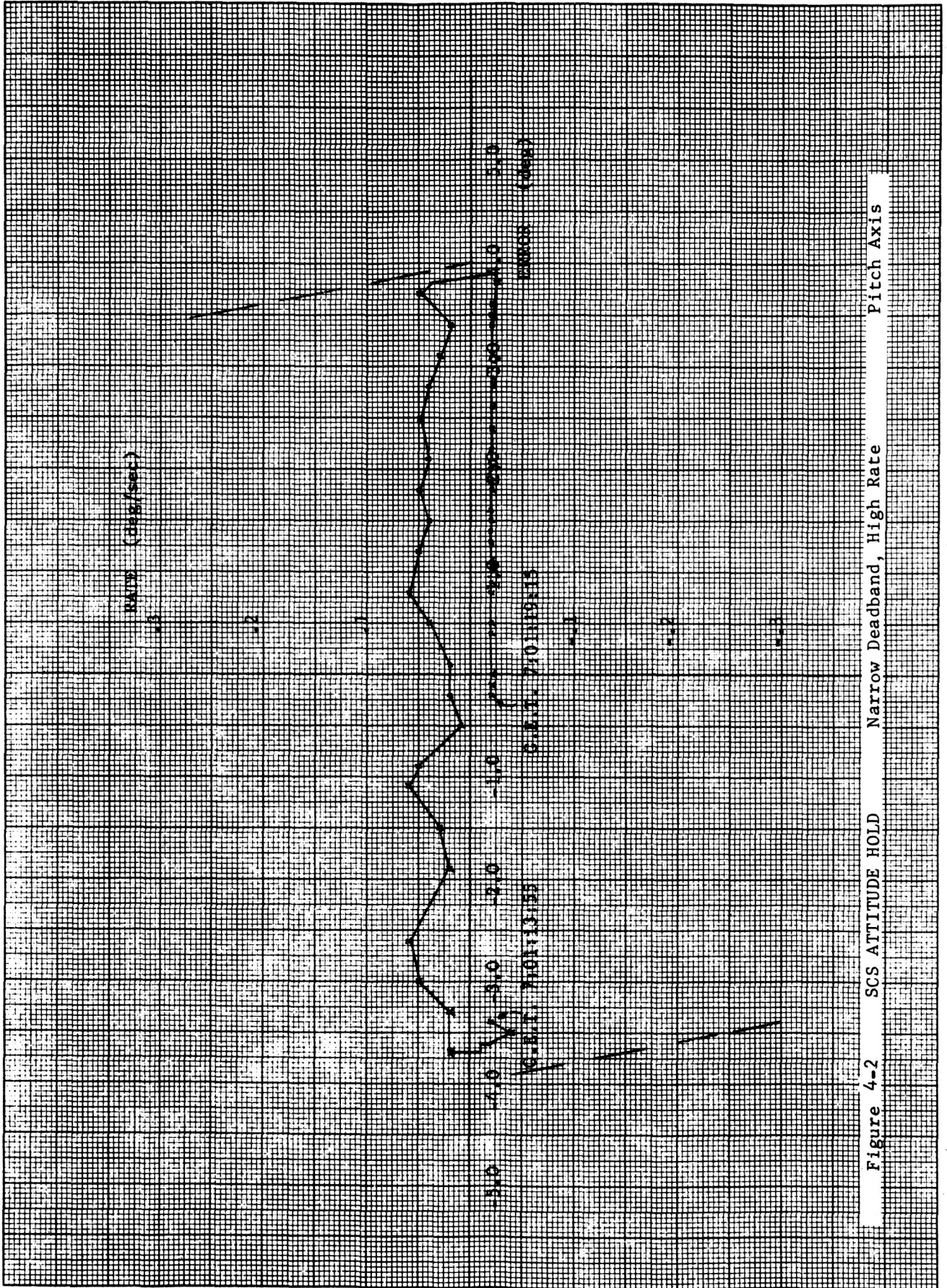
Figure 4-2   SCS ATTITUDE HOLD   Narrow Deadband, High Rate   Pitch Axis
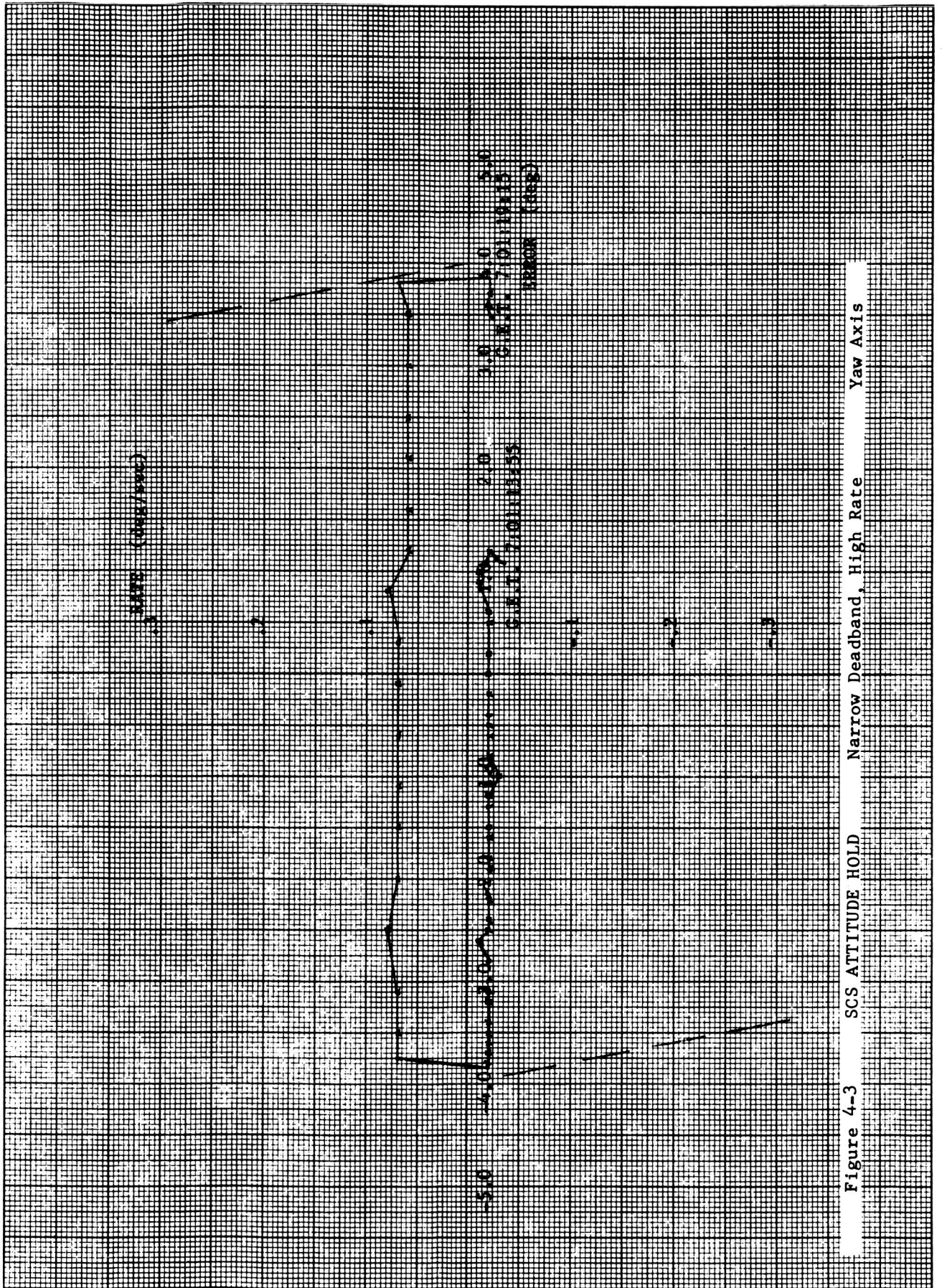
Figure 4-3   SCS ATTITUDE HOLD   Narrow Deadband, High Rate   Yaw Axis

Table 4-I—Attitude Errors for SPS Burns

SPS Burn No.	Ullage Peak		Rate	Ignition Attitude			Burn Peak Attitude			Final Attitude		
	P	Y	R	P	Y	R	P	Y	R	P	Y	R
1. GεN	-.42	-.08	-.26	-.84	+.27	-.10	+.19	+.27	-3.35	-.07	-.28	-3.35
2. GεN	-.34	+.32	+.22	-.84	-.20	+.54	-.17	+.27	-1.72	+.15	-.20	-1.72
3. SCS	-.14	-.16	+.14	+.03	-.04	-.02	+.70	+.98	+.06	+.66	+.12	+.06
4. GεN	-.30	+.16	+.06	-.72	+.90	+.38	-.09	-.28	-.27	-.09	-.28	-.27
5. GεN MTVC	-.34	+.32	+.26	-.96	+.90	+.54	-.17 / +.55	+.37 / -1.22	-5.38 / +2.76	-.02 / +.23	-.24 / -.51	+1.97 / -1.92
6. GεN	-.42	-.28	+.10	-.80	-.39	+.38	-.08	-.04	-.18	-.08	-.04	-.18
7. SCS	-.03	+.12	+.08	+.48	+.21	-.40	+.86	+1.03	-.14	+.52	+.04	+.06
8. GεN	-.54	+.24	+.22	-.84	-.16	+.54	-.19	+.43	-3.19	-.01	-.32	-3.19

Table 4-II - SPS Burn Data

SPS Burn No.	Tracking Station and Rev.	Ullage				Burn	
		No. Jets	Start GET	Duration	Overlap	Start GET	Duration
1. GεN	Canarvon 17	4	26:24:41.47	15.7	1.5	26:24:55.67	9.4
2. GεN	Canarvon 18	4	28:00:43.78	14.2	1.5	28:00:56.47	7.8
3. SCS	Canarvon 48	4	75:47:45.54	5.76	0.0	75:48:00.27	9.3
4. GεN	Texas 76	2	120:42:41.25	20.8	1.6	120:43:00.45	0.5
5. GεN MTVC	Mila 105	2	164:59:40.93	21.2	1.5	165:00:00.46	66.9
6. GεN	Mila 132	2	210:07:42.23	19.9	1.7	210:07:59.99	0.5
7. SCS	Antigua 151	4	239:05:58.75	13.95	1.3	239:06:11.41	8.3
8. GεN	Hawaii Entry	4	259:39:02.34	16.5	1.5	259:39:16.36	10.9

Burn durations and overlap are given in seconds. GET is in hr:min:sec.

Table 4-III - Engine Gimbal Trims

Pitch Angle-degrees

SPS Burn No.	RO3 Display		Initial Trim		Single-shot		Final Value		Mistrim
	First	Final	PACTOFF	measured	PACTOFF	Change	PACTOFF	measured	
1. GεN	-.85	-.90	-.9015	-.86	-.8067	+.0948	-.8304	-.68	-0.1
2. GεN	-.90	-.86	-.8541	-.81	-.8541	0.	-.8541	-.81	0.0
3. SCS			-.8541	-.90	none	none	SCS	-.68	-0.2
4. GεN			-.8541	-.81	none	none	-.8541	-.90	0.0
5. GεN	-.78	-.78	-.7829	-.73	-.7829	0.	-.7118	-.64	0.0
MTVC			-.7118	-.64	none	none	SCS	-.64	takeover
6. GεN			-.7355	-.68	none	none	-.7355	-.68	0.0
7. SCS	-.74	-.74	-.7355	-.88	none	none	SCS	-.68	-0.2
8. GεN			-.7355	-.68	-.7355	0.	-.7355	-.68	0.0

Yaw Angle-Degrees

SPS Burn No.	RO3 Display		Initial Trim		Single-shot		Final Value		Mistrim
	First	Final	YACTOFF	measured	YACTOFF	Change	YACTOFF	measured	
1. GεN	-.31	-.31	-.3084	-.22	-.1661	+.1423	-.1898	-.22	-0.1
2. GεN	-.31	-.40	-.4034	-.31	-.2610	+.1424	-.3044	-.35	-0.1
3. SCS			-.4508	-.48	none	none	SCS	-.35	-0.1
4. GεN			-.6457	-.44	none	none	-.6457	-.98	0.0
5. GεN	-.50	-.50	-.4982	-.39	-.3798	+.1184	-.7355	-.69	-0.1
MTVC			-.7355	-.69	none	none	SCS	-1.07	takeover
6. GεN			-1.2611	-1.15	none	none	-1.2611	-1.19	0.0
7. SCS	-1.30	-1.30	-1.3049	-1.15	none	none	SCS	-.95	0.0
8. GεN			-1.3049	-1.19	-1.1625	+.1424	-1.2811	-1.32	-0.1

and TVC DAP errors were less than half a degree. During ullage, the RCS DAP permitted attitude errors to build up to nearly one degree, but the SCS held attitude to less than half a degree at SPS ignition. A list of these attitude errors for all the SPS burns appears in Table 4-I along with peak attitude rates during ullage and the end-of-burn attitude errors. The data indicates no malfunctions in either the SCS or Digital Autopilots.

RCS DAP performance was remarkably consistent throughout the six G&N controlled ullages. Pitch attitude errors at ignition were expected to "hang off" outside the negative deadband at roughly the same value for all burns during Mission C because of the constant c.g. offset in the pitch plane. The 4-jet ullages (Burns 1, 2 and 8) yielded identical attitude errors and the 2-jet ullages for Burns 4, 5 and 6 varied only slightly. Yaw attitude errors at ignition were within the +0.5 degree deadband except for the 2-jet ullages. Roll firings during ullage were few and of short duration.

TVC DAP attitude errors were very small for all DAP controlled burns. Peak attitude errors were larger in yaw because initial engine mistrims were larger. Final attitude errors in yaw result from a lag in the c.g-tracking loop which estimates trim changes at half-second intervals. During the fifth SPS burn, the roll error exceeded the five degree deadband and the TVC Roll DAP commanded one short roll jet firing of 0.210 second duration with two jets. No other TVC DAP roll firings were required during the mission.

Slosh oscillations dominated the attitude rate and engine angle traces in the oscillographs for most of the burns but was almost completely absent in some cases. Burns 1 and 8 were nearly free of slosh oscillations. Burn 3 produced an oscillation in pitch rate of ± 0.7 deg/sec, but had no evident of yaw sloshing. Burn 5 exhibited pitch and yaw slosh effects due to manual inputs as well as initial conditions.

Manual takeover during Burn 5 produced very small engine angle transients which were detected at the time of takeover. These transients were small and short-lived indicating a smooth switching in gimbal drives when the hand controller was activated. Crew reports, confirmed by body rate data, indicate MTVC operation was excellent.

4.3.2 Durations and GET Times for SPS Burns

Tracking stations, ignition times and burn durations for the SPS burns and the corresponding ullage maneuvers are given in Table 4-II. All times are Ground Elapsed Time (GET) and are based upon solenoid bilevel states which do not included delays in thrust buildup and decay. Ullage overlap refers to the length of time between the SPS engine-on command and the end of ullage. During Burn 3 ignition the engine was commanded on at the same time that the ullage was terminated with no adverse effect on ignition.

Manual takeover during Burn 5 occurred at GET 165:00:35.78 after 35.32 seconds of G&N control. Manual rate control was used for the remaining 31.58 seconds of the burn.

All the burns exhibited the same gimbal position transients at ignition and termination. At ignition, the pitch gimbal moved sharply positive by about 0.25 deg, the yaw gimbal moved negative about 0.5 deg, and then both gimbals returned to the initial trim position. At thrust termination the transients were near mirror images of ignition transients, but were much smaller in amplitude. These transients are attributed to thrust misalignment and gimbal compliance acting on the actuator during thrust buildup and tail-off.

4.3.3 Engine Gimbal Trim Angles

A preliminary list of engine gimbal trim values has been tabulated from Computer Word data at times near SPS burns. Two CMC variables referred to as PACTOFF (pitch trim) and YACTOFF (yaw trim) represent the computer estimate of the trim thrust deflection required to compensate for c.g. offset and other thrust alignment variables. A list of values for PACTOFF and YACTOFF before and during each SPS burn are given in Table 4-III.

Normally, before each burn, Routine 03 is performed to check on engine trim angles and other DAP variables. The astronaut has the option to change these variables at any time. The first two columns of the table labeled "R03 Display" give the initial and final values indicated by a NOUN 48 in the Major Modes tab group of the Computer Words data for the four cases so far discovered.

The actual values of PACTOFF and YACTOFF are given at ignition, after the single-shot correction (TIG+3.7 sec) and at the end of each G&N burn. The measured gimbal angles are also given in the table at ignition and cutoff for each burn. For G&N controlled burns the listed values for PACTOFF and YACTOFF should be comparable to the measured gimbal angles; for SCS controlled burns, the desired gimbal angles are entered manually via thumbwheels and PACTOFF and YACTOFF are not used. The bias between PACTOFF and the pitch gimbal angle measurement was consistently 0.05 degree, and the yaw bias averaged 0.09 degree but was highly variable. The crew apparently attempted to bias the PACTOFF value before the first burn and the YACTOFF value before the second burn in order to obtain the desired gimbal angles on the Gimbal Position Indicator (GPI) which displays the measured gimbal angles. Results indicate that the original values were better and that the biases introduced by the crew had no effect on TVC performance. Burns 4 and 6 were only half-second burns and Burn 5 was divided between computer and SCS control.

After each burn, the values for PACTOFF and YACTOFF reverted to their preburn values which indicates no automatic updates were made for the next burn.

Mistrims were small, probably less than 0.2 degree for all burns. These mistrims can be estimated by the size of the single-shot correction during a G&N controlled burn as indicated by the table. Such small mistrims would not be expected to provide much challenge to either the TVC DAP or the pilot in controlling the spacecraft.

4.4 ENTRY DAP PERFORMANCE EVALUATION

A brief chronological description of the reentry is presented, comparing the actual entry to preflight simulation results. The bank angle response to commands from guidance was investigated and the history of the jet firings for rate damping in the pitch and yaw axes was examined in detail. RCS propellant usage during reentry was determined on a per axis basis, and contrasted to simulation results.

CM/SM separation occurred at 259:43:32.2 GET and the CM was placed under SCS minimum impulse control with the A and B rings enabled.

At 259:43:47.5 GET the 45 degree yaw amneuver to entry attitude was performed. This maneuver and the subsequent 140 degree pitch maneuver to entry attitude appeared nominal. The B ring was disabled at 259:45:46.1 GET and minimum impulse control with the A ring was utilized. The roll maneuver to bring the CM "heads down" was performed at 259:49:32.5 GET during which time minimum impulse controlled the dynamic coupling arising in the pitch and yaw axes. Minimum impulse control was operative for several minutes following the roll maneuver and on several occasions, attitude excursions were intentionally induced by commanding a series of minimum impulse firings. These excursions were nulled by subsequent minimum impulse firings. These exercises served to determine the spacecraft response in the MIC mode. At 259:55:40.7 GET 0.05 g was sensed and 0.2 g was sensed at 259:55:06.7 GET. These events were evidenced by the program changes occurring in the CMC. It should be noted here that although the DAP was not in control of the spacecraft, the DAP was initialized and program switchovers were made. A roll maneuver to a bank angle of -55 degrees was performed at 259:56:13 GET.

Control of the CM changed from SCS to CMC at 259:57:29.6 GET and the bank angle was automatically driven to -70 degrees by the Entry DAP. Figure 4-4 illustrates the CMC roll commands and actual roll attitude during reentry. Five major bank angle maneuvers were commanded by entry guidance for cross-axis steering. During major roll maneuvers, the DAP correctly accelerated the roll rate to the maximum maneuver rate of 20 degrees/second. Correct jet on-time calculation by the DAP was demonstrated by the DAP's ability to null both the roll attitude error, $R-R_c$, and the roll rate. On the first roll maneuver, which was performed single-ring, a small attitude overshoot occurred at the end of the maneuver with no rate overshoot. This characteristic appeared in preflight simulations. On subsequent roll maneuvers, which were performed dual-ring, rate overshoots of two to three degrees per second occurred at the end of the maneuver. This is to be expected from dual ring operation since the second jet on-time computation within the two-second Roll DAP is computed assuming single-ring operation. The ability of the DAP to

4-12
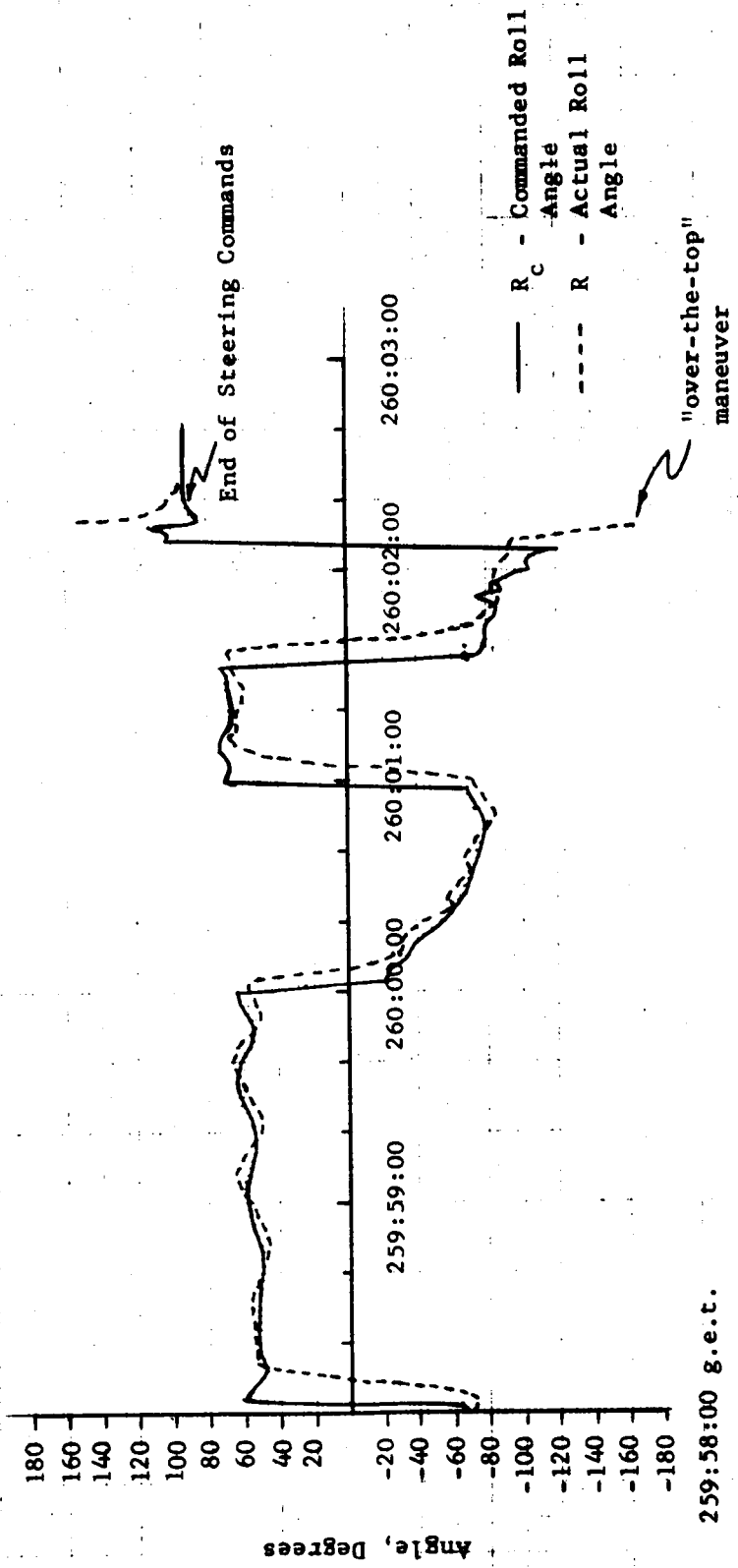
Figure 4-4

Commanded and Actual Roll Angles During Reentry

compute the shortest angular path was demonstrated by the maneuver at 260:02:10 GET where the DAP correctly executed an "over-the-top" maneuver.

At 259:58:30.1 GET, the B-ring was enabled and both the A and B rings were utilized during the remainder of the reentry phase. The reason for this switch was an angular disturbance during which time the commander thought the pitch rate was becoming excessive. Examination of the data during this time period revealed a jump in the pitch and yaw rates at 259:58:14.3 GET; however, the change in pitch rate was approximately 1.2 degrees per second while the change in yaw rate was .8 degrees per second. No jets were firing at this time and approximations of the pitch and yaw disturbing accelerations yielded -8 degrees/second^2 and -10 degrees/second^2, respectively. The cause of these accelerations are unexplained; however, no jet firing were required to control the resultant rates and no stability problem was encountered.

An investigation of the time histories of the relative pitch and yaw rates during the period of CMC control indicated smooth response until approximately 260:01:35 GET. Prior to this time, rate damping within the prescribed two degree per second deadbands was achieved by single 100 ms pulses of the two ring system. The frequencies of oscillation of these rates compared well with the values determined by preflight simulations.

The spacecraft velocity at 260:01:48 GET was approximately Mach 1.6 and aerodynamic effects became quite noticeable thereafter. Indeed, RCS jet firings for rate damping became more frequent and of longer duration (multiples of 100 ms). The degree of increased jet activity during the transonic phase of reentry is reflected in the breakdown of RCS propellant consumption during reentry shown in Table 4-IV. A total of 18.22 pounds of propellant was expended for pitch and yaw axis control from the time of CM/SM separation. Two-thirds of this total was expended in the last two minutes of reentry. The total RCS propellant expenditure of 47.14 pounds exceeded the expected consumption based on preflight simulation results. Several factors contributed to this difference. The number of bank angle reversals exceeded the number required in the simulations. The actual reentry utilized both the A and B rings while the simulated reentry was for single-ring control.

4-14

Table 4-IV - RCS Propellant Consumption

Time	Event	Pitch Axis*		Yaw Axis*		Roll Axis*	
		System A	System B	System A	System B	System A	System B
259:43:33.2	CM/SM Separation	0	0	0	0	0	0
260:01:48	Mach 1.6	2.08	0.95	1.65	1.38	14.48	6.94
260:03:20.4	Auto Disable of Jets	5.24	4.11	4.61	4.26	18.23	10.69

*Consumption value represents expenditure from time of CM/SM separation.

Also, no preflight simulations have produced the response exhibited during the transonic phase where high jet activity was experienced. It should be noted that the "rough" behavior during the transsonic phase was also exhibited in the reentries of spacecrafts 017 and 020. The models of aerodynamics in the transsonic region as used in the entry simulators for preflight did not adequately describe the actual environment and propellant expenditures based on these simulations were low. Postflight simulation runs which incorporated the measured wind profiles with the aerodynamic model yielded results comparable to flight conditions.

Examination of the rate gyro data during entry indicated possible incompatibility with the RCS jet activity. However, the CMC utilizes rate estimates instead of rate gyro data for determining jet firings. Hence, to resolve the differences between the rate gyro data and the CMC rate estimates, a reconstruction of the CMC DAP compuations was performed. To effect a detailed DAP analysis, certain variables were required which were not included in the downlink data. The Entry DAP routine "CM/POSE" was duplicated utilizing as input variables the telemetered data, $\underline{R}_N$, MVREL, CDU and the REFSMMAT matrix. The variables obtained were the Euler angles R, β, and α, the roll attitude about the realtive velocity vector, the sideslip angle and the angle of attack respectively, which measures the CM attitude relative to the entry relative velocity vector, and γ, the angle between the local horizontal and the relative velocity vector. The data used in the reconstruction was available to two-second intervals via the downlink and the CMC incorporates corrections to the computations to account for changes within the two-second period. This updating was not utilized in the reconstruction of "CM/POSE" but comparisons of the computed roll angle R to the value of R telemetered by the CMC were good. The rate estimator values of p, q, and r, the angular rates about the body X, Y, and Z axes, are incorporated with values of α, R, and γ to create the set, prel, qrel, and rrel, the angular rates about the entry (wind) coordinate axes.
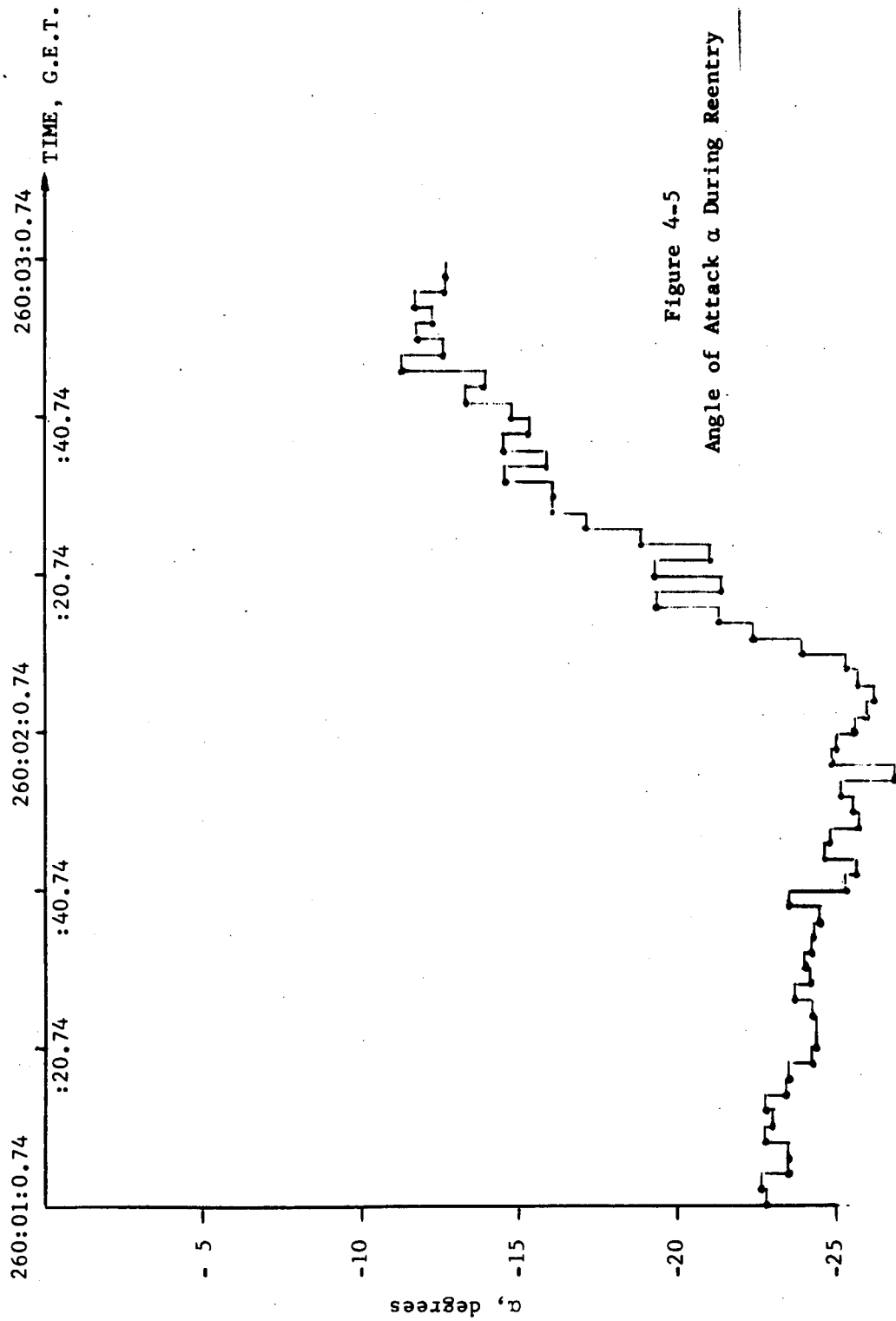
Figure 4-5

Angle of Attack α During Reentry

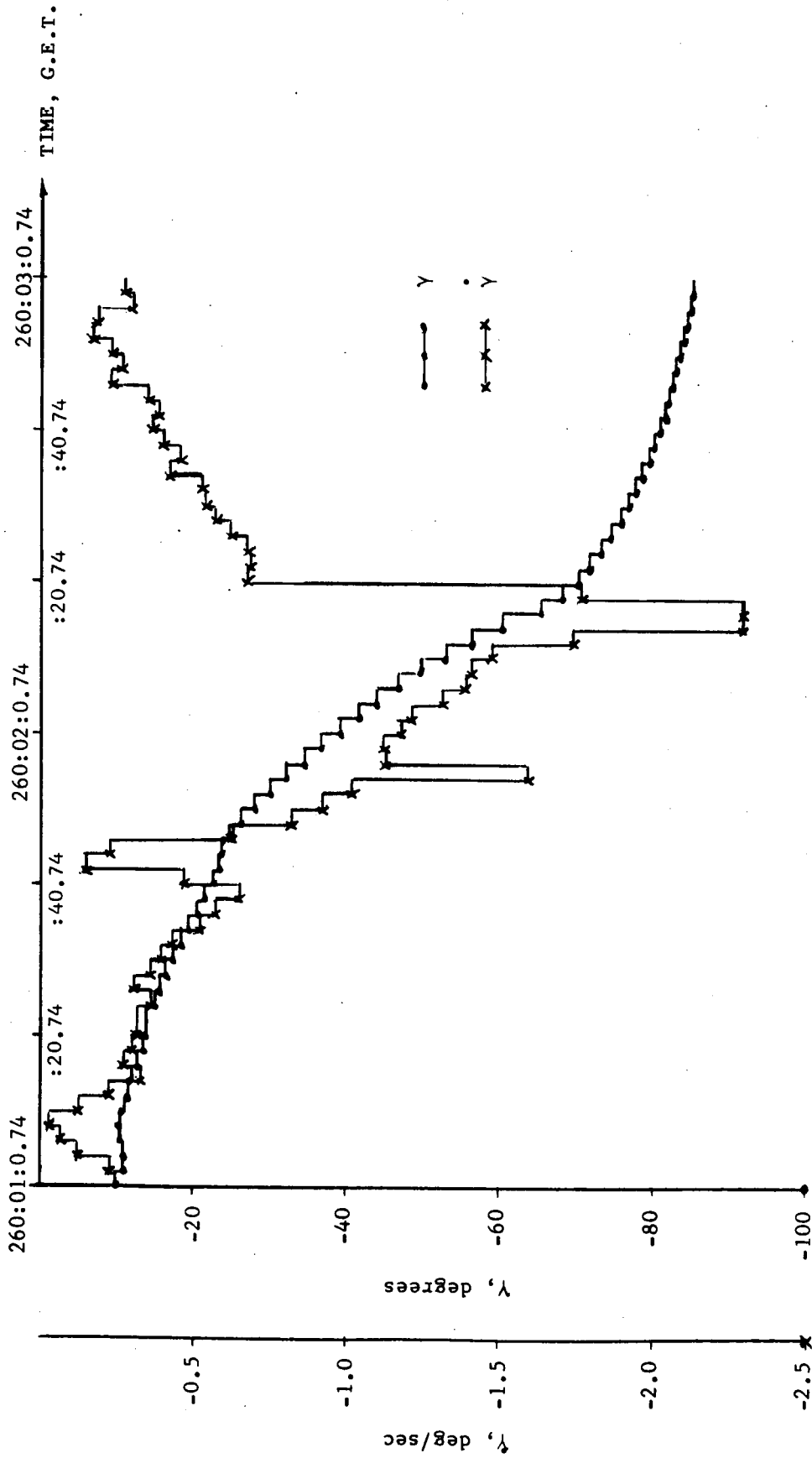Figure 4-6

γ and $\dot{\gamma}$ During Reentry

During the atmospheric phase of reentry, the Entry DAP maintains the rates, qrel and rrel-(prel·tanα) with the deadbands of $\pm$ 2 degrees per second.

Oscillograph records were available during reentry which provided information from the rate gyros. The analog signals defined the pitch and roll rates and the relative yaw rate was computed as r-p tan α_c by passing the yaw and roll rate-gyro outputs through appropriate circuitry. It should be noted that these analog signals did not compensate for the effect of $\dot{\gamma}$ as is done in the Entry DAP and computation of the relative yaw rate is based on a fixed values of α_c, the nominal angles of attack used in the SCS entry rate measurement circuitry. Attempts were made computed values with these two factors. The time history of the angle α is given in Figure 4-5 while Figure 4-6 represents the time histories of γ and $\dot{\gamma}$.

The oscillograph records revealed that, at times, pitch or yaw jets were fired when the rate gyro signals indicated that the relative rates were within the prescribed deadbands. On infrequent occasions, no jets were fired when the rate was outside the deadband. However, since the Entry DAP uses the rate estimator output to activate the jets, the rate estimator values for the relative pitch and yaw rates were superimposed on time plots of the rate gyro outputs in Figures 4-7, 4-8 and 4-9. Although the Entry DAP generated rate estimates every 100 ms, telemetry data provided the values every 200 ms. Hence, only half of the estimator values were available for investigation which precluded a conclusive analysis. In Figure 4-7, several + pitch firings occurred even though the analog pitch rate remained within the -2 degrees per second deadband. The rate estimator output validated two of these firings by virtue of the fact that the estimator values were outside the deadband at the times of the jet firings. Another estimator value appeared to be at the deadband, but the time of its occurrence did not correspond exactly to the time of the jet firing. However, as noted previously, only half of the estimator values are available and rate estimates could
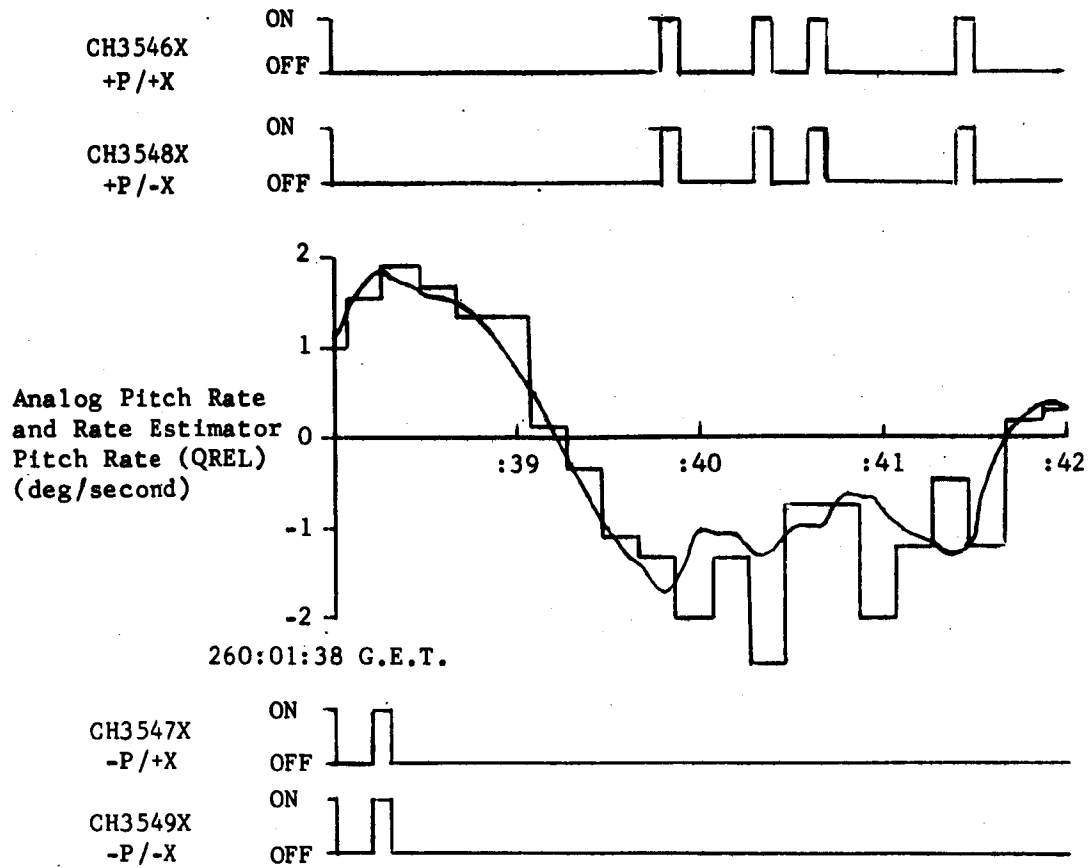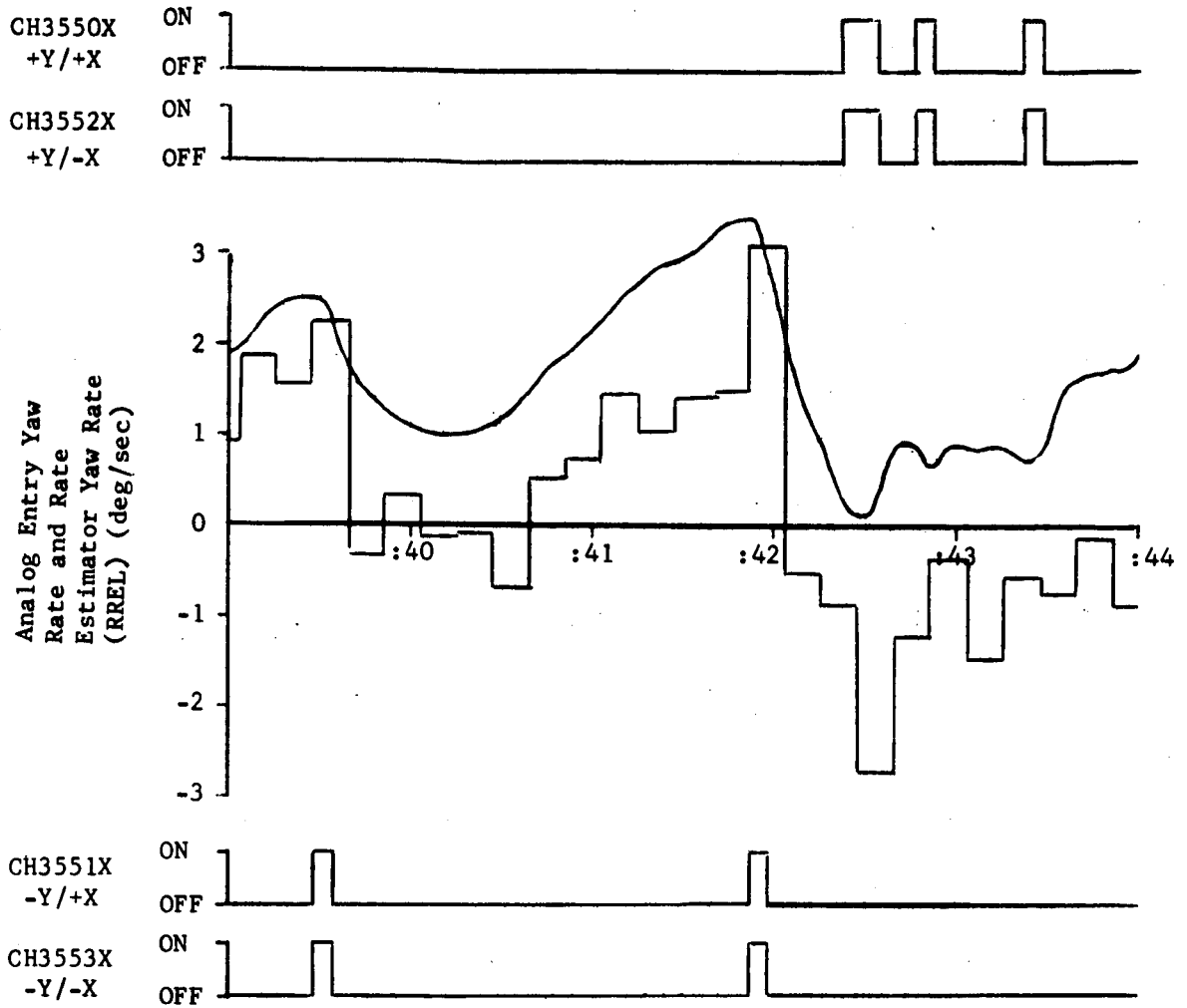
CH3546X
+P/+X
ON
OFF

CH3548X
+P/-X
ON
OFF

Analog Pitch Rate
and Rate Estimator
Pitch Rate (QREL)
(deg/second)

2

1

0

:39   :40   :41   :42

-1

-2

260:01:38 G.E.T.

CH3547X
-P/+X
ON
OFF

CH3549X
-P/-X
ON
OFF

FIGURE 4-7

Time Histories of Analog QREL,
Rate Estimator QREL, and CM RCS Jet Firings

260:01:38 GET to 260:01:42 GET

4-20

FIGURE 4-8

Time Histories of Analog RREL,
Rate Estimator RREL, and CM RCS Jet Firings
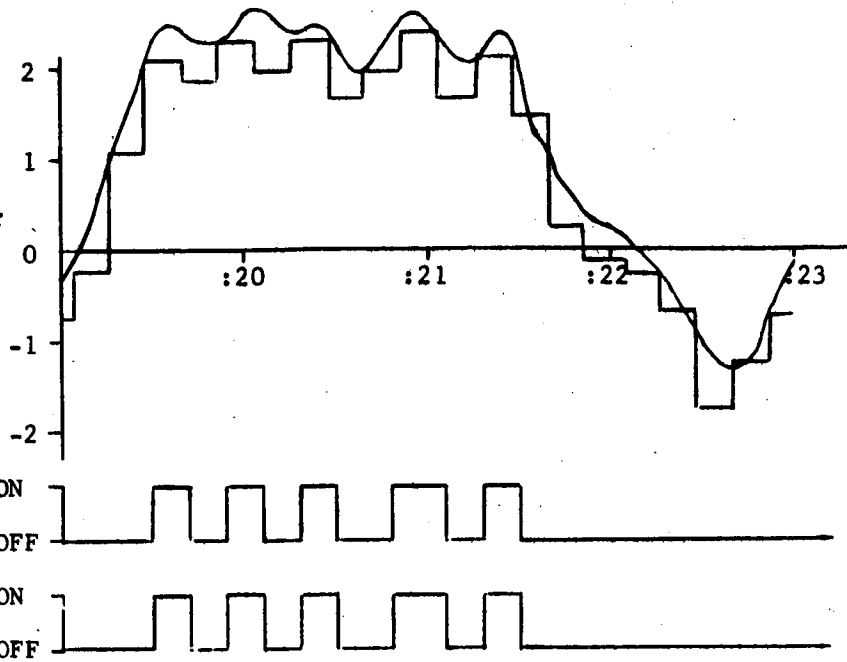
260:01:39 GET to 260:01:44 GET

4-21

FIGURE 4-9

Time Histories of Analog QREL,
Rate Estimator QREL, and CSM RCS Jet Firings

260:02:19 GET to 260:02:23 GET

have existed which caused the third and fourth + pitch firings shown
in Figure 4-7. The rate estimate which did not have a corresponding
jet firing only approached the rate deadband and the DAP may have
interpreted the value as being within the deadband. Part of the
differences between the analog signal and the estimator values could be
attributed to the $\dot{\gamma}$ effect. The Entry DAP does not compensate for the
effect until $\dot{\gamma}$ exceeds 0.5 degrees per second. As indicated in Figure
4-6, $\dot{\gamma}$ did exceed this value for this period of time.

Examination of the rate gyro values for the relative yaw rate shown
in Figure 4-8 caused some concern since + yaw jets were fired when the
analog rate was positive. However, the rate estimates during that time
were negative; indeed, one of the + yaw firings was substantiated by a
rate estimator value. Again, lack of data precluded definite verification
of the other two firings. Figure 4-8 indicates significant differences
between the analog values for rrel and the rate estimator values. Again,
$\dot{\gamma}$ exceeded 0.5 degrees per second and was incorporated in the DAP
computations. Also, the use of a fixed value for α_c in the formation
of rrel from the rate-gyro outputs could cause significant differences
since rrel is quite sensitive to α variations.

Figure 4-9 illustrates the pitch rate response during the transonic
phase of reentry. An important observation is that although the -pitch
firings did reverse the pitch acceleration and drive the pitch rate back
within the rate deadband (on the basis of rate estimator values), aero-
dynamics effects counteracted this effect. The pitch rate was driven
back beyond the deadband and a series of -pitch firings resulted before
the rate was completely reversed. This behavior was not duplicated in
any preflight simulations; that is, in the simulations, single firings
were sufficient to completely reverse the rate. Hence, the predicted
propellant consumption would definitly be lower than the actual expen-
diture. In Figure 4-9 all of the firings were substantiated by rate
estimator values. Whereas the analog signal remained outside the dead-
band despite jet firings, the rate estimator values toggled about the

Although the rate gyros and the IMU are both subjected to vibration
during reentry, their locations within the CM structure cause some
differences in the amplitudes and frequencies of the vibrations applied
to the individual pieces of equipment. Also, it is known that during
periods of high roll rate (greater than four degrees per second) the
CDU switches between a high and low-rate sampling frequency which can
create errors as high as one degree per second.

The Entry DAP control of the CM about the roll axis appeared nominal
both for single and the dual-ring control. On the basis of partial data,
rate damping in the pitch and relative yaw axes appeared nominal although
complete verification was not possible. The multiple firings were not
DAP induced but were environment related. Several factors, such as $\dot{\gamma}$
effects, α effects, vibrations, and CDU errors could contribute to the
differences between the rate-gyro outputs and the rate estimator out-
puts. Perhaps the most significant conclusion of this analysis is
that existing entry simulations are inadequate in modeling the transonic
aerodynamics. For propellant consumption estimates to be useful for
flight planning these models must be accurately defined and the influence
of transonic aerodynamics on propellant consumption clearly defined.
deadband. From Figure 4-6, it is noted that $\dot{\gamma}$ was greater than 0.5
degrees per second during this time period and the Entry DAP performed
as designed and it was disturbing torque effects which caused the multiple
firings.

The time periods depicted in Figures 4-7, 4-8 and 4-9 were selected
because they were representive of the erratic response experienced
during the transonic phase of reentry. The available data indicates
that the DAP performed well and differences between the rate-gyro
outputs and the rate estimator values may generally be attributed to
$\dot{\gamma}$ and α effects. Two other potential sources for the differences in
the gyro and estimator values are structural vibrations and CDU errors.

APPENDIX A

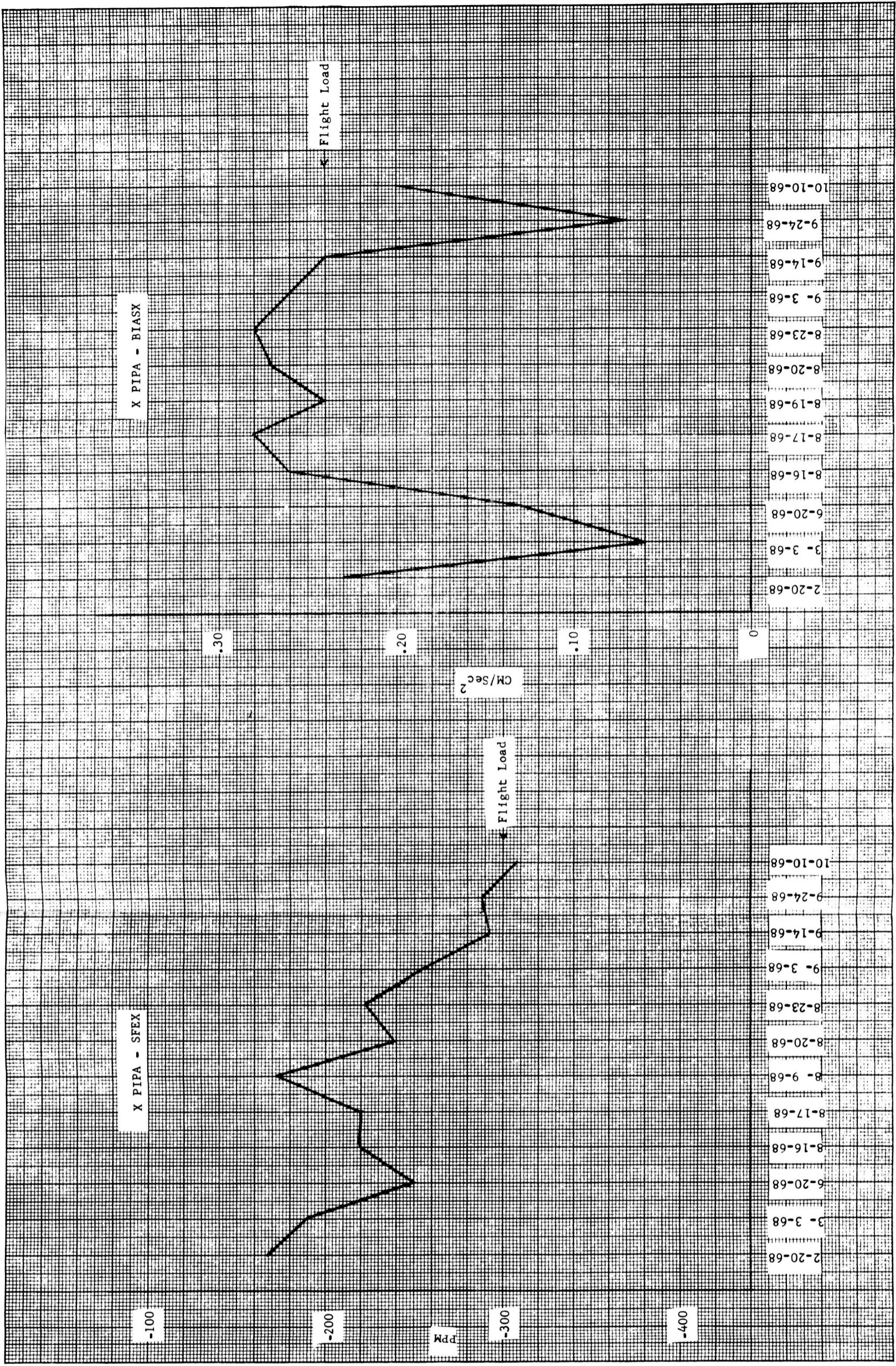## PREFLIGHT CALIBRATION TIME HISTORIES

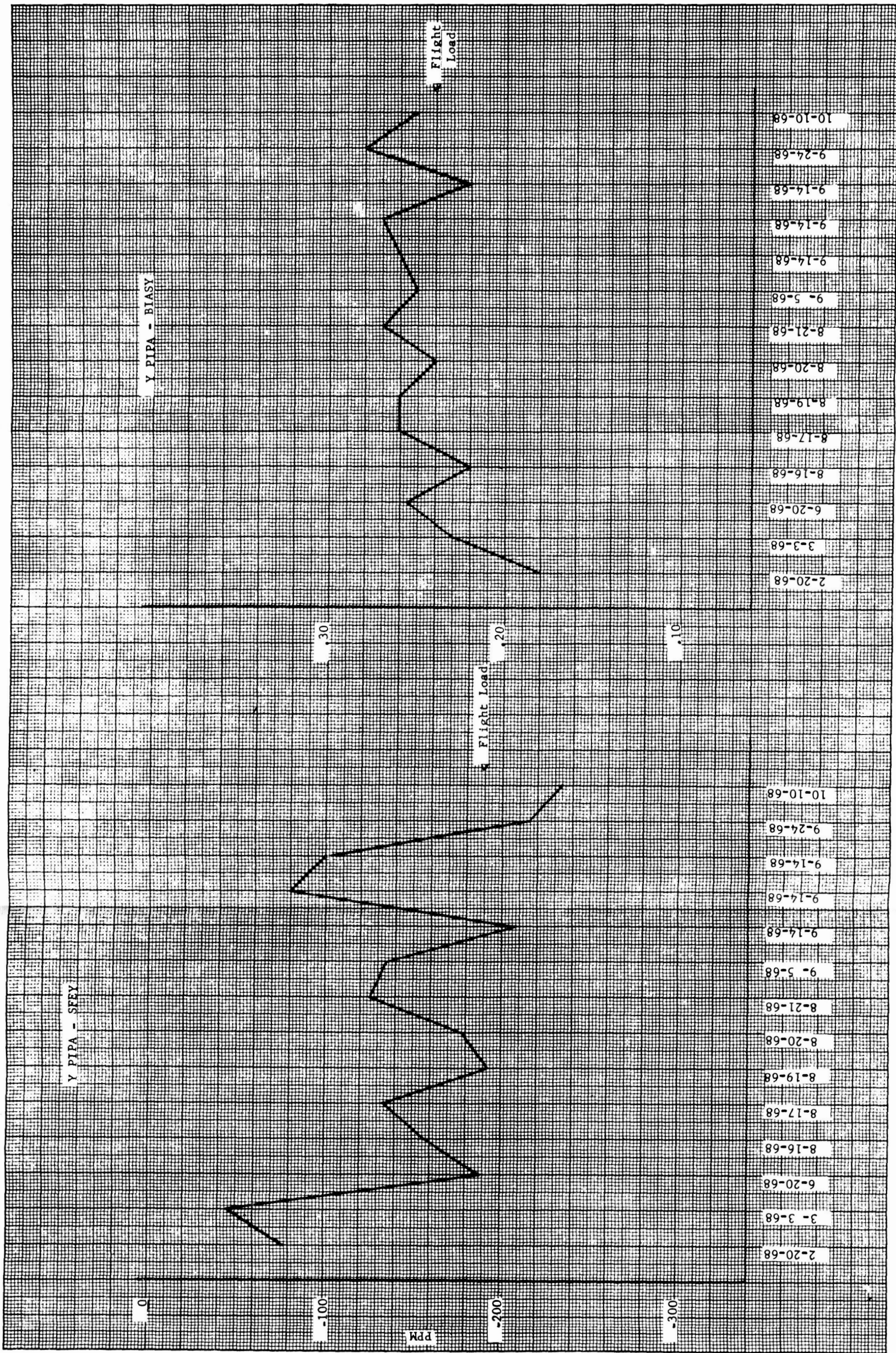Figure A-1
XPIPA Calibration Time History
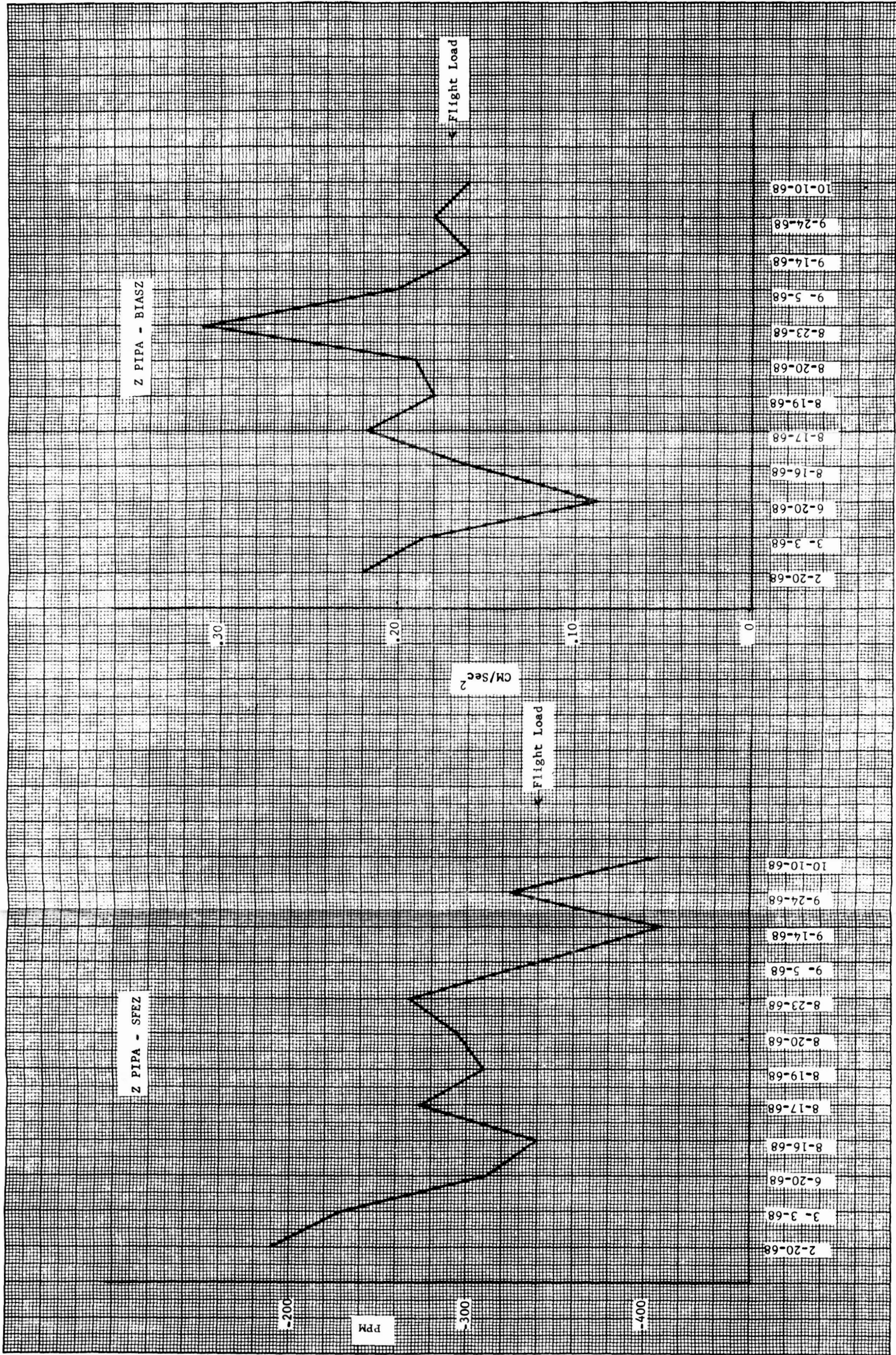
Figure A-2
YPIPA Calibration Time History
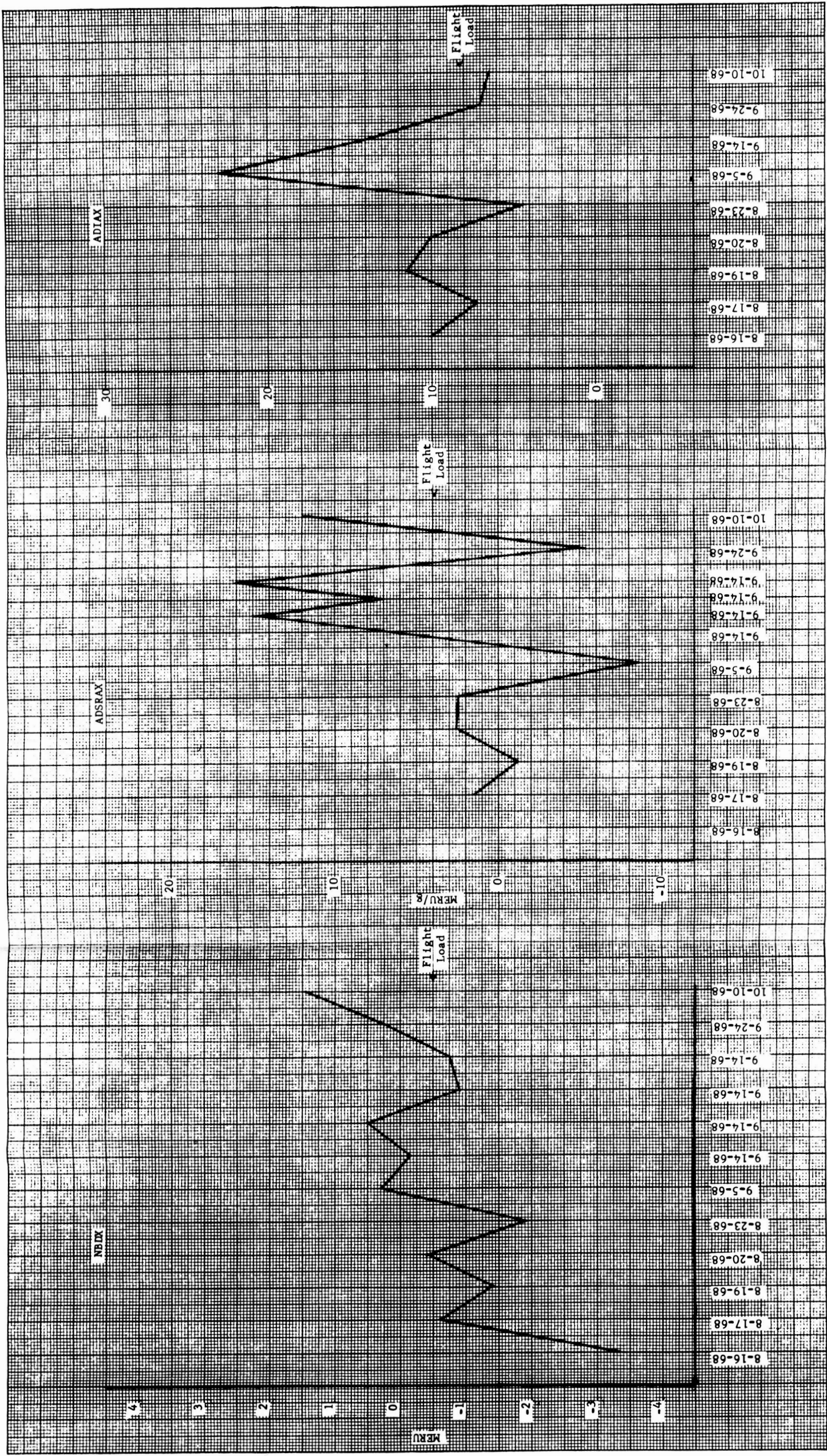
Figure A-3

ZPIPA Calibration Time History

Figure A-4

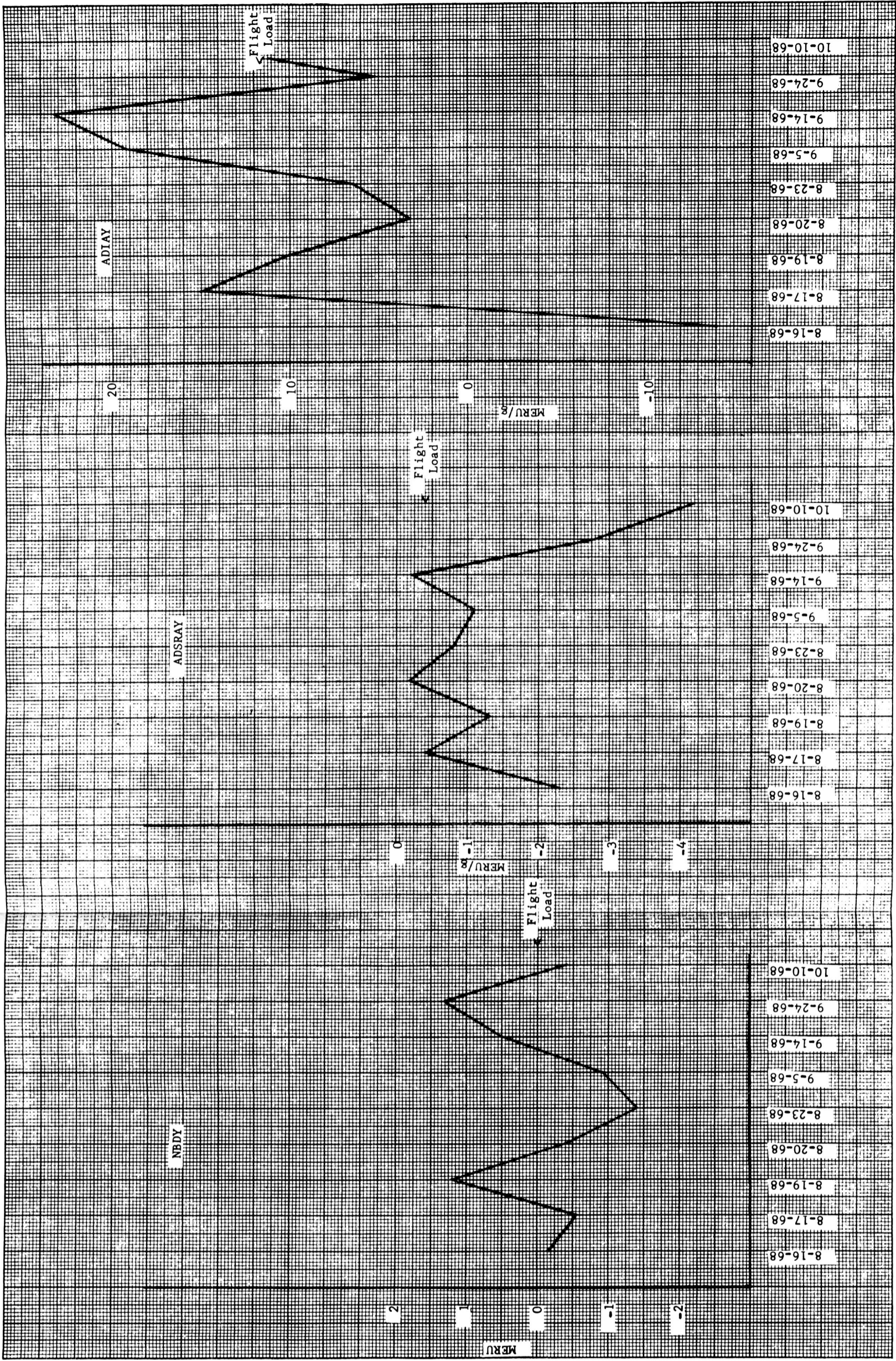X IRIG Calibration Time History
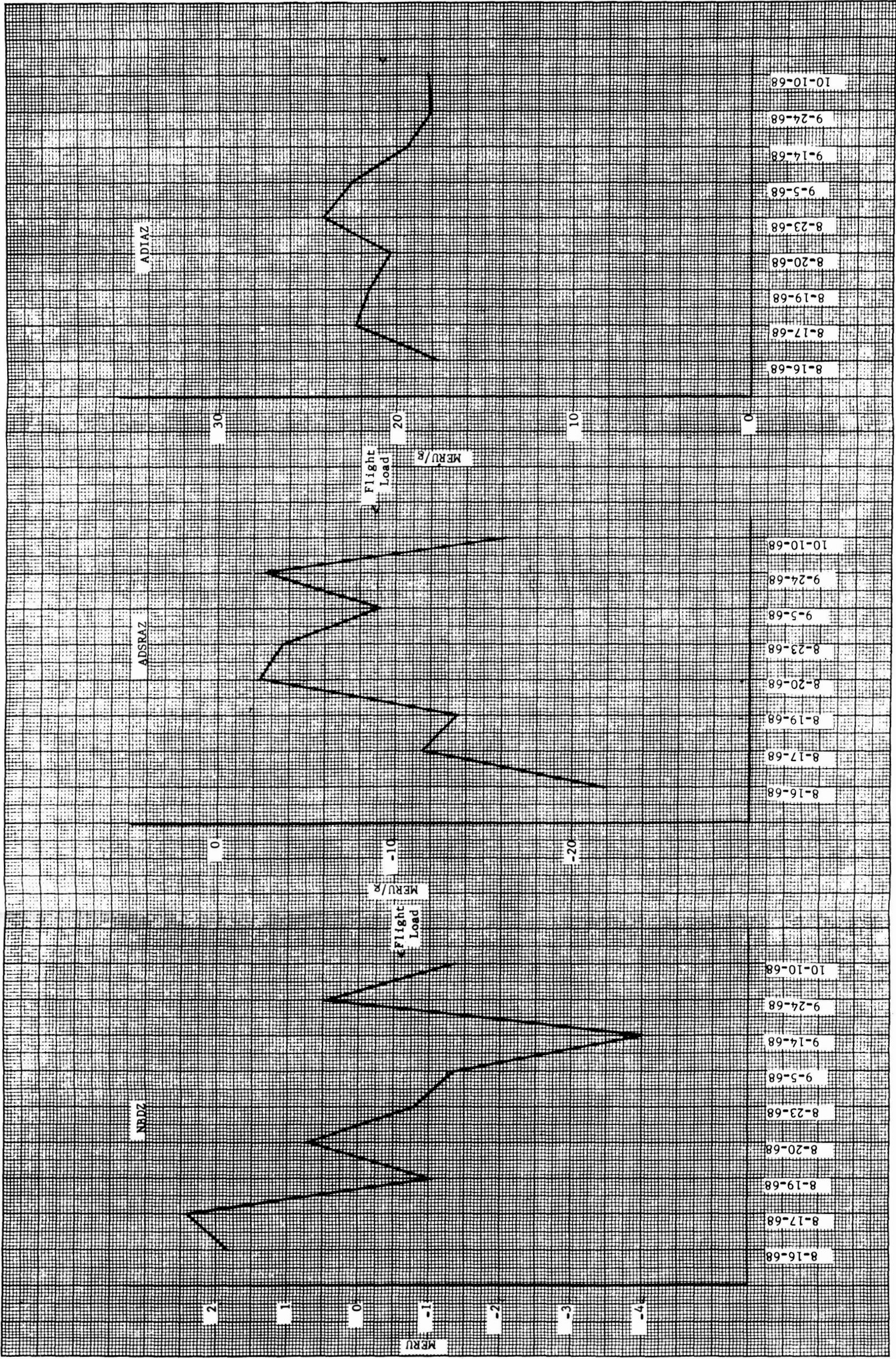
Figure A-5
Y IRIG Calibration Time History

Figure A-6

Z IRIG Calibration Time History

APPENDIX B

ANALYTIC METHODOLOGY

APPENDIX B

METHODOLOGY

1. METHODOLOGY

1.1 Trajectory Reconstruction

There are two available measures of G&N performance which have cardinal significance in the spacecraft (S/C) postflight error analysis. During non-G&N controlled mission phases (GRR and Boost through Coast: S-IVB attached), the measurement of greatest significance is the accuracy with which the S/C IMU and CMC sense and record actual trajectory parameters. During G&N controlled phases, focus shifts to a measure of the accuracy with which targeted trajectory parameters (the nominal trajectory) are attained by the spacecraft. For both situations, reliable knowledge of the actual trajectory is an essential tool. To this end, analysis is centered on a reconstructed, best estimate trajectory (BET). This trajectory was obtained via a working interface between this task and Task A-50 (Trajectory Reconstruction, MSC/MPAD). The reconstruction and related error analysis proceed as follows.

a) Basic Data Processing and EAP

Before trajectory reconstruction or IMU error analysis can be undertaken, the basic data tapes must be edited and processed so that they are compatible with the trajectory computing programs. The configuration for the processing of the basic data sources, and the production of an EAP tape, is shown in Figure B-1. This is a straightforward procedure, and the function of each of the four programs involved is explained in the following subsections.

b) G&N Processor Program

The G&N Processor reads total position, total velocity, incremental PIPA counts, and time ($\vec{P}_T$, $\vec{V}_T$, ΔN, t) from the input CMC telemetry tape. The program editing capability provides for correcting data in individual records, deleting records, inserting new records, and reconstructing lost data by interpolating between the values of $\vec{P}_T$ and $\vec{V}_T$ bounding the specified dropout interval.
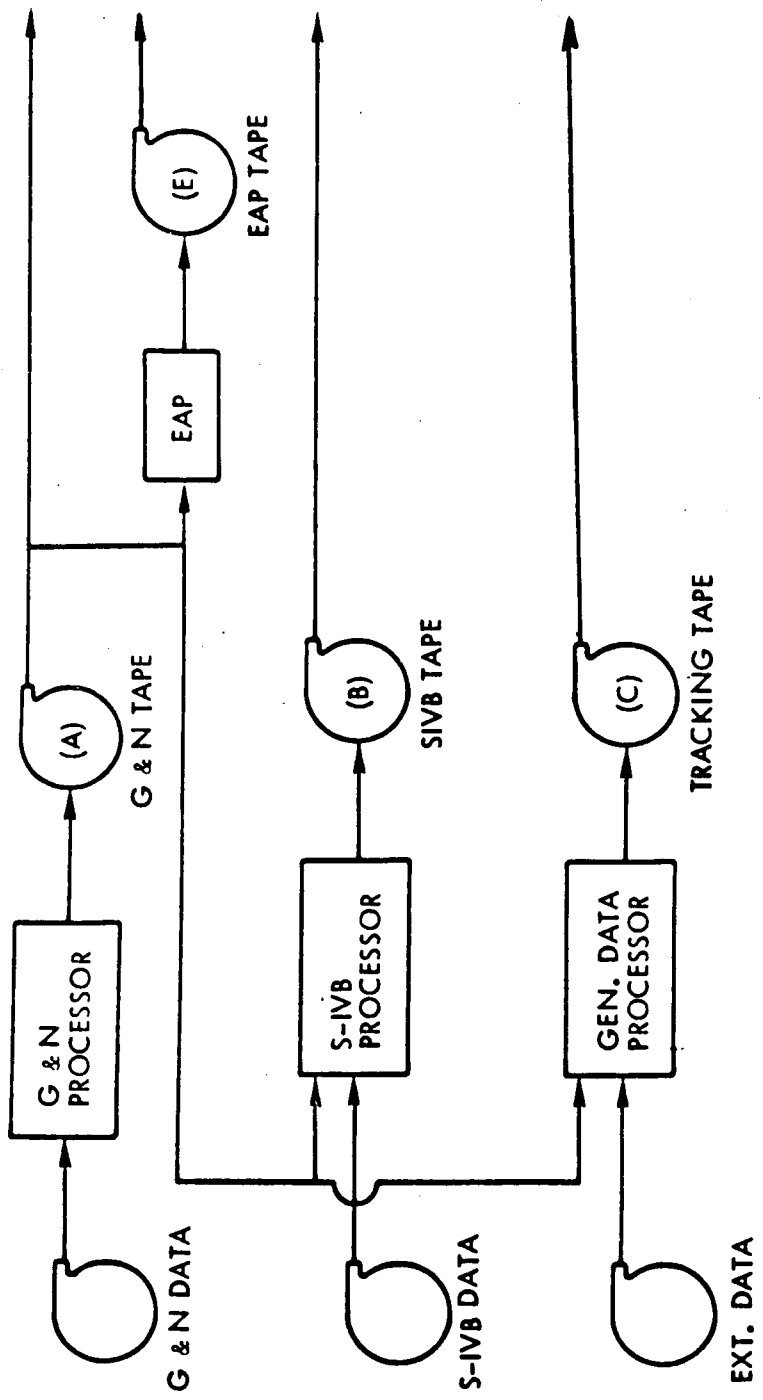
Figure B-1. Configuration for Processing Basic Data Sources

Processing of the edited data proceeds in two phases:

1) Phase I

    The incremental PIPA counts, ΔN, are used to compute sensed position, velocity, and acceleration ($\vec{P}_s$, $\vec{V}_s$, $\vec{A}_s$). The desired values of each PIPA scale factor and bias may be loaded into the program for this computation. Total position and velocity are rotated into ECIG coordinates.

2) Update Phase

    If desired, a total position and velocity may be specified at any time in the trajectory, and the program will re-compute the trajectory from this "update state vector" and the incremental PIPA counts. This capability is useful for reconstructing short burns. The following quantities are computed:

    a) $\vec{P}_T$, $\vec{V}_T$ in G&N coordinates

    b) $\vec{P}_T$, $\vec{V}_T$, $\vec{A}_T$ in ECIG coordinates

    c) $\vec{G}$ - acceleration due to gravity in G&N coordinates.

c) S-IVB Processor Program

    The S-IVB Processor reads sensed velocity and acceleration, total inertial position and velocity, and time

$\vec{V}_s$(S-IVB), $\vec{A}_s$(S-IVB), P_T(S-IVB), V_T(S-IVB), t(S-IVB)

    from the S-IVB telemetry tape, and G&N time, T_{GN}, from the G&N coordinate frame and interpolated to the G&N time base. The time history (G&N time) of the following quantities are computed:

    1) $\vec{V}_s$, $\vec{A}_s$ in G&N coordinates

    2) $\vec{P}_T$, $\vec{V}_T$ in G&N coordinates

    3) $\vec{P}_T$, $\vec{V}_T$ in ECIG coordinates

d) General Data Processor Program

    The General Data Processor, as used in Apollo postflight evaluation, reads position and velocity (usually RAE or XYZ surface fixed) and time from a tracking data tape,

B-3

and G&N time from the G&N processor tape. The tracking data is transformed into a Cartesian coordinate frame and interpolated to the G&N time base. The output tape contains the following trajectories in the G&N time base.

1) Total position, velocity, and acceleration in ECIG coordinates.

2) Position, velocity, and acceleration in the tracking system coordinates.

c) Position, velocity, and acceleration in an ESF coordinate frame (ENU or Downrange-Crossrange-Up).

e) Apollo IMU Error Analysis Program (EAP)

The EAP Program reads sensed acceleration, $\vec{A}_s$, in guidance coordinates, and time, T, from the G&N processor tape. The output program is position and velocity error partial derivatives (in guidance coordinates) with respect to each of 40 IMU error sources. These error sources are defined in Table B-1.

If the guidance coordinates are not coincident with the accelerometer coordinates, $\vec{A}_s$ is rotated into accelerometer coordinates, and acceleration errors, $\partial\vec{A}/\partial e_i$, are computed for each of the 40 error sources, e_i. These acceleration errors are then trapezoidally integrated to obtain velocity and position errors which are rotated back into guidance coordinates and written on the output tape. The values of each e_i are input to any of the programs which employ an EAP output to construct a corrected trajectory.

f) Boost Phase Trajectory Reconstruction

The configuration for computing corrected G&N trajectories, and comparing G&N with other trajectory data is shown below and in Figure B-2.

The Velocity Comparison Program (VELCOMP) corrects the G&N trajectory using the EAP partials and the values of IMU errors input by load sheet. The corrected G&N trajectory is differenced in both sensed and total "coordinates" with either S-IVB or high speed tracking data.
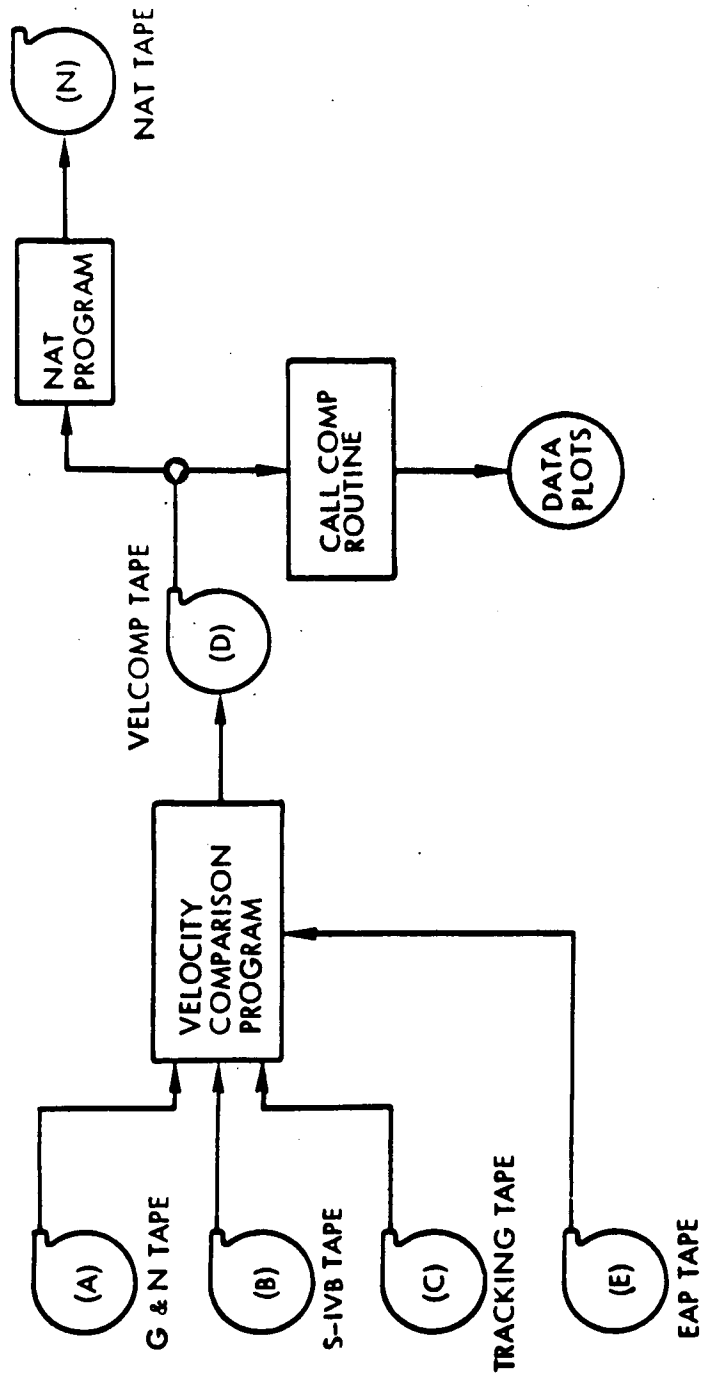
B-4

Figure B-2. Configuration for Correcting, Comparing and Analyzing Boost Guidance Data

B-5

The configuration of Figure B-2 can also be used to reconstruct burns, provided accurate, high speed position data is available throughout the burn.

The VELCOMP program may be used in several configurations (selected by load sheet options) in correcting and reconstructing the G&N trajectory. The following diagram shows the general configuration.
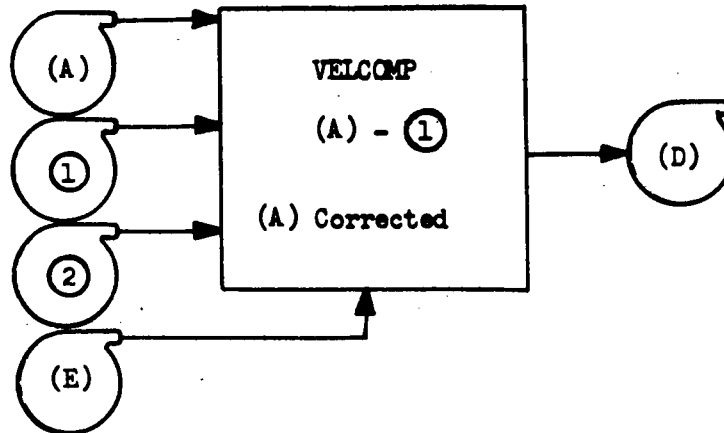
A minimum of two tapes are required as input.

- (A) - Sensed position and velocity and total position and velocity (P_s, V_s, V_T) in G&N coordinates are read from the G&N Processor output.

- ① - The tape ① may be an output from either the S-IVB Processor or the General Data Processor. The program reads total position and velocity in ECIG coordinates from this tape.

Generally, an EAP output, (E), will also be included, in which case the program reads the position and velocity partials for each of the IMU error sources. The values of the errors themselves are input to the VELCOMP program via load sheet.

If neither of the tapes (A) or ① being compared contains accurate position information, another tape, ②, may be input. The program reads total position in ECIG coordinates from this tape and uses this information only in computing the gravity profile.

B-6

In the discussion of the computations made by the VELCOMP program, the following notation will be used:

$\vec{P}$, $\vec{V}$ are position and velocity data from the G&N tape;

$T\vec{P}$, $T\vec{V}$ are position and velocity data from tape ①;

M is the matrix which transforms from ECIG to G&N coordinates;

$\vec{P}_I$, $\vec{V}_I$ are initial conditions in ECIG coordinates.

Each of the following quantities are computed and written on the VELCOMP output tape.

Guidance Computations

$$[\delta \vec{P}_s]_{G\&N} = \sum_i \frac{\partial \vec{P}_s}{\partial e_k} e_k$$

$$[\delta \vec{V}_s]_{G\&N} = \sum_i \frac{\partial \vec{V}_s}{\partial e_k} e_k$$

Gravity Profile

$[\vec{P}_G, \vec{V}_G, \vec{A}_G]_{ECIG}$ - These quantities are computed from total position data on any of the tapes, (A), ①, ②, for any specified segment of the trajectory. The gravity model assumes the Fisher Ellipsoid.

"Tracking" Data (Tape ①) in Sensed Coordinates

$$[T\vec{P}_S, T\vec{V}_S]_{G\&N} = M \left| [T\vec{P}_T, T\vec{V}_T]_{ECIG} - [\vec{P}_G, \vec{V}_G]_{ECIG} \right.$$

$$\left. - [\vec{P}_I, \vec{V}_I]_{ECIG} \right|$$

"Tracking" Data (Tape ①) in Total Coordinates

$$[T\vec{P}_T, T\vec{V}_T]_{G\&N} = M [T\vec{P}_T, T\vec{V}_T]_{ECIG}$$

B-7

Sensed Position and Velocity Comparison

Note: Let the compensated G&N data be represented by

$$\vec{P}_s{}' = \vec{P}_s - \delta\vec{P}_s \qquad \vec{V}_s{}', \ \vec{V}_s{}' = \vec{V}_s - \delta\vec{V}_s$$

$$[\Delta\vec{P}_s, \ \Delta\vec{V}_s]_{G\&N} = [\vec{P}_s{}', \ \vec{V}_s{}']_{G\&N} - [T\vec{P}_s, \ T\vec{V}_s]_{G\&N}$$

Total Position and Velocity Comparison

Note: "Compensated" total G&N data is defined by

$$\vec{P}_T{}' = \vec{P}_T - \delta\vec{P}_s \qquad \vec{V}_T{}' = \vec{V}_T - \delta\vec{V}_s$$

$$[\Delta\vec{P}_T, \ \Delta\vec{V}_T]_{G\&N} = [\vec{P}_T{}', \ \vec{V}_T{}']_{G\&N} - [T\vec{P}_T, \ T\vec{V}_T]_{G\&N}$$

Delta of Delta Comparison

$$[\Delta^2\vec{P}, \ \Delta^2\vec{V}]_{G\&N} = [\Delta\vec{P}_T, \ \Delta\vec{V}_T]_{G\&N} - [\Delta\vec{P}_s, \ \Delta\vec{V}_s]_{G\&N}$$

Reconstructed G&N Trajectory

The total corrected G&N trajectory in ECIG coordinates is computed from

$$[\vec{P}_{TC}, \ \vec{V}_{TC}]_{ECIG} = M^{-1} [\vec{P}_s{}', \ \vec{V}_s{}']_{G\&N} + [\vec{P}_G, \vec{V}_G] + [\vec{P}_I, \ \vec{V}_I]$$

g) Orbital Maneuver Reconstruction

Since continuous (and accurate) high speed tracking is
not expected during the orbital maneuvers, the con-
figuration of Figure B-2 cannot be used to compensate
and reconstruct the G&N trajectory. The trajectory
reconstruction program has the capability of recon-
structing an entire G&N trajectory using only sensed
velocity (and EAP partials) as an input. The configu-
ration for reconstructing burns (and entry if applicable)
is shown in Figure B-3.

If tracking is available over segments of a burn,
position and velocity comparisons may be generated
with the VELCOMP program using the configuration
shown in Figure B-3. The Trajectory Reconstruction
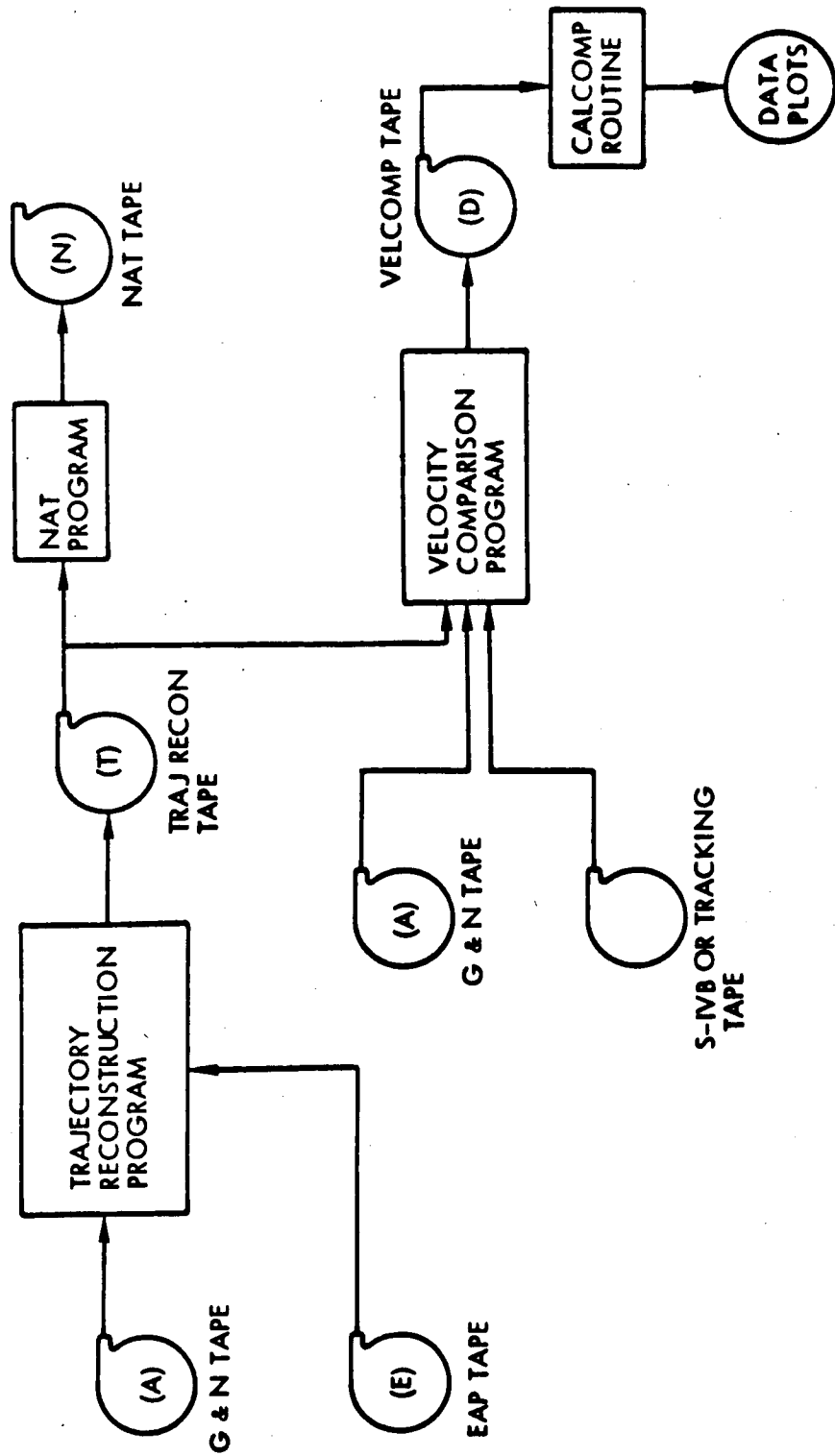Program output (which contains corrected total position

B-8

Figure B-3. Configuration for Correcting, Comparing and Analyzing Burn Data

data) is used to generate the gravity profile, and the comparisons are made as explained earlier.

The trajectory reconstruction program utilizes two input tapes: sensed velocity is read from the G&N processor tape; $\partial V_s / \partial e_k$ is read from the EAP tape.

The error magnitudes, e_k, initial position and velocity, P_I and V_I in ECIG coordinates, and the Matrix, M, which transforms from ECIG to G&N coordinates are input to the program via load sheet.

The program output consist of the following quantities:

● $P_T \quad V_T \quad A_T$ in ECIG coordinates. This is the reconstructed trajectory which is computed as follows: The sensed velocity corrections are computes from

$$\delta V_s = \sum_k \frac{\partial V_s}{\partial e_k} e_k$$

Total velocity at time "i" is computed from

$$V_{Ti} = V_I + M^{-1} (V_{Si} - \delta V_{Si}) + V_{Gi}$$

Where $V_{Gi} = V_{Gi-1} + \dfrac{A_{Gi-1} + A_{Gi}}{2}$ and

$$A_{Gi} = A_{Gi} (P_{Ti-1} \cdots P_{Ti-4})$$

Total position is computed from $P_{Ti} = P_I + \dfrac{V_{Ti-1} + V_{Ti}}{2} \delta t$

Total acceleration is computed from $A_{Ti} = \dfrac{V_{ti} - V_{Ti-1}}{\delta t}$

● P_T, V_T rotated into G&N coordinates.

● Several NAT output quantities, viz., Nos. 9, 10, 11, 12, 13, 14, 15, 16, 19, 20, 21, 50 - 55.

B-10

h) NAT Program

The NAT (NASA Apollo Trajectory) Program accepts
the output tapes from the G&N Processor, VELCOMP
Program, Trajectory Reconstruction Program, and
ESPOD. The program also accepts input tables of
atmospheric data which is used for computation during
entry. The output tape contains 112 parameters which
are listed in the NAT Index.

1.2 IMU Evaluation

The VELCOMP program was a basic tool used in arriving at a set
of "most probable" IMU errors. Trial values of the error quantities were
loaded into this program and the output for each trial was examined for
conformance with the BET. That set of errors which reduced the "cor-
rected" G&N trajectory residuals to a minimum for all accurate BET inter-
vals was postulated as the most probable set of error values. Prelaunch
G&N calibration data provided a source of most probable errors for initial
trial values. Subsequent trial errors were selected based upon an exami-
nation of the preceding VELCOMP position and velocity residuals (deltas
with respect to the BET). A final most probable set of error values was
obtained from the earlier estimates using a Kalman filter technique.

The boost phase of any mission is most important for determining
IMU errors because acceleration levels are high and good high speed
tracking is available. For this reason, comparisons of "corrected"
(trial) G&N trajectories with the boost phase BET will yield the most
reliable estimates of IMU errors.

2. ESPOD

As will be noted, the principal source referred to for trajectory
data during coasting phases of the flight is ESPOD. ESPOD denotes
"Editing and Special Perturbation Orbit Determination. " This program
is a comprehensive model of the principal and perturbing accelerations
which act on a vehicle during free fall (non-thrusting, exo-atmospheric
flight). As such, it is used to generate a continuous estimate of the free
fall trajectory of an orbiting spacecraft based upon radar data and models
of the earth's potential field, aerodynamic drag, lunar, solar, and plan-
etary perturbations, and radiation pressure.

Accelerometer Errors		Gyro Errors	
VOX VOY VOZ	Velocity Offset (CM/sec)	NBDX NBDY NBDZ	Constant drift rate (meru/g)
ACBX ACBY ACBZ	Bias (CM/sec^2)	ADIAX ADIAY ADIAZ	Drift rate sensitivity to acceleration along input axis (meru/g)
SFEX SFEY SFEZ	Scale Factor (parts/million, ppm)	ADSRAX ADSRAY ADSRAZ	Drift rate sensitivity to acceleration along spin axis (meru/g)
NCX NCY NCZ	SF sensitivity to input acceleration squared (ppm/g)	ADOAX ADOAY ADOAZ	Drift rate sensitivity to acceleration along output axis (meru/g)
XICRO YICRO ZICRO	SF sensitivity to coupling of acceleration along input and output axes (ppm/g)	A^{2}DIAX A^{2}DIAY A^{2}DIAZ	Drift rate sensitivity to acceleration squared along input axis (meru/g^2)

		Platform Errors	
MXAZ MXAY MYAZ MYAX MZAY MZAX	MIAK is the misalignment of accelerometer "I" input axis about the "K"th platform axis. Sign convention is positive when misalignment reduces the angle between the positive axes. (arc-sec)	MLMX MLMY MLMZ	Platform misalignment (arc-sec)
		DT	Timing error (sec)